Metal-Organic Frameworks for Drug Delivery: A Design Perspective

Harrison D. Lawson^{1,3}, S. Patrick Walton^{1*}, and Christina Chan^{1,2*}

- (1) Michigan State University, Department of Chemical Engineering and Materials Science, 428 S. Shaw Lane, East Lansing, Michigan 48824, United States
- (2) Michigan State University, Department of Biochemistry and Molecular Biology, 603 Wilson Road, East Lansing, Michigan 48824, United States
- (3) Carnegie Mellon University, Department of Chemical Engineering (Current Affiliation), 5000 Forbes Avenue, Pittsburgh, Pennsylvania 15213, United States

*Corresponding Author(s):

(517) 432-1105 FAX

S. Patrick Walton
Department of Chemical Engineering and Materials Science
Michigan State University
428 S. Shaw Lane, Room 3249
Engineering Building
East Lansing, MI 48824-1226
spwalton@egr.msu.edu
(517) 432-8733

Christina Chan
Department of Chemical Engineering and Materials Science
Michigan State University
428 S. Shaw Lane, Room 1243
Engineering Building
East Lansing, MI 48824-1226
krischan@egr.msu.edu
(517) 432-4530
(517) 432-1105 FAX

Author(s):

Harrison Lawson
Department of Chemical Engineering
Carnegie Mellon University
5000 Forbes Avenue
Doherty Hall
Pittsburgh, PA 15213-3815
hlawson@andrew.cmu.edu
https://orcid.org/0000-0002-0946-2354

Keywords: *Metal-organic frameworks; Biomolecules; Drug loading; Structure; Synthesis;* Characterization; Biocompatibility; Cellular targeting

Abstract

The use of metal-organic frameworks (MOFs) in biomedical applications has greatly expanded over the last decade due to the precision tunability, high surface areas, and high loading capacities of MOFs. Specifically, MOFs are being explored for a wide variety of drug delivery applications. Initially, MOFs were used for delivery of small-molecule pharmaceuticals; however, more recent work has focused on macromolecular cargos, such as proteins and nucleic acids. Here, we review the historical application of MOFs for drug delivery, with a specific focus on the available options for designing MOFs for specific drug delivery applications. These options include choices of MOF structure, synthetic method, and drug loading. Further considerations include tuning, modifications, biocompatibility, cellular targeting, and uptake. Altogether, this review aims to guide MOF design for novel biomedical applications.

Abbreviations

BIOLOGICAL TEST SYSTEM

BIOLOGICAL TEST SYSTEM	
293T	Human embryonic kidney
3T3	Swiss albino mouse embryo fibroblast
4T1	Mouse mammary carcinoma
A2780	Human ovarian carcinoma
A2780/CDDP	Human ovarian carcinoma cisplatin resistant
A549	Human adenocarcinoma alveolar basal epithelial cells
APC	Antigen-presenting cell
B16-F10	Murine skin melanoma
BT-474	Human mammary ductal carcinoma
BXPC-3	Human pancreatic carcinoma
CACO-2	Human colorectal epithelial adenocarcinoma
CAD	Murine catecholaminergic neuronal tumor
CHO	Chinese hamster ovary
COS7	Monkey kidney fibroblast-like cell
DC2.4	Murine dendritic cell
H460	Large cell lung carcinoma
HACAT	Human keratinocyte
HASMC	Human aortic smooth muscle cells
HDF	Human dermal fibroblasts
HEK-293	Human embryonic kidney
HEKN	Human epidermal keratinocytes neonatal
HELA	Human cervical cancer adenocarcinoma
HEPG2	Human hepatocellular carcinoma
HL-60	Human promyelocytic leukemia
HL7702	Human liver cell
HMSC	Human mesenchymal stem cell
HT-29	Human colorectal adenocarcinoma
HUVEC	Human umbilical vein endothelial cell
J774.A1	Murine monocyte macrophage
L02	Human liver cell
L929	Murine fibroblasts
MC3T3	Murine osteoblast precursor
MCF-10A	Human pre-neoplastic mammary epithelial cells
MCF-7	Human breast adenocarcinoma
MCF-7/T	Human breast adenocarcinoma taxol resistant
MDA-MB-231	Human epithelial breast cancer
MDA-MB-468	Human pleural effusion metastatic breast cancer
MGC-803	Human gastric mucinous adenocarcinoma
MH-S	Murine alveolar macrophages
NCI-H292	Human lung carcinoma
NIH-3T3	Murine embryonic fibroblasts
NOD/SCID MICE	Nonobese diabetic/severe combined immunodeficiency mice
PBL	Human peripheral blood lymphocytes
PBMC	Human peripheral blood mononuclear cells
PC-12	Rat pheochromocytoma
PC-3	Human prostate adenocarcinoma
RAW264.7	Murine macrophage
RBC	Red Blood Cell
SH-SY5Y	Human neuroblast
SK-BR-3	Human breast adenocarcinoma
SKOV3	Human ovarian adenocarcinoma
SMMC-7721	Human hepatocellular carcinoma
SW480	Human colorectal adenocarcinoma
T1D RAT	Type 1 diabetes rat
THP-1	Human monocyte (acute monocytic leukemia)
U 937	Human histiocytic lymphoma
U-87	Human glioblastoma
U-01	Truman gnoblastoma

CARGO

ALPHA-CHC	A-cyano-4-hydroxycinnamic acid
BETA-GAL	Beta-galactose
BSA	Bovine serum albumin
CPG	5'—C—phosphate—G—3'
CYT C	Cytochrome C
GFP	Green Fluorescent protein
GMP	Gemcitabine monophosphate
HRP	Horse radish peroxidase
HSA	Human serum albumin
MP-11	Microperoxidase-11
OVA	Ovalbumin
PQQ-GDH	Glucose dehydrogenase
RAPTA-C	Ru(n ⁶ -p-cymene) Cl₂(PTA)
RNASE A-NBC	Ribonuclease A ROS responsive modification
SBHA	Suberohydroxamic acid
SOD	Superoxide dismutase
VEGF	Vascular endothelial growth factor

MOF

HUSKT	Hong Kong University of Science and Technology
IRMOF	Isoreticular MOF
MIL	Matériaux de l'Institut Lavoisier
MIP	Materials of the Institute of Porous Materials of Paris
NCP	Nanoscale coordination polymer
NU	Northwestern University
PCN	Porous coordination network
UIO	Universitetet i Oslo
UMCM	University of Michigan Crystalline Material
ZIF	Zeolitic imidazolate framework
ZJU	Zhejiang University

VIABILITY TESTS

CCK8	Cell Counting Kit-8
MTT	3-(4,5-dimethylthiazol-2-yl)-2,5-diphenyltetrazolium bromide
MTS	3-(4,5-Dimethylthiazol-2-yl)-5-(3-carboxymethoxyphenyl)-2-(4-sulfophenyl)-2H-tetrazolium
SRB	Sulforhodamine B
WST	Water Soluble Tetrazolium Salts
LDH	Lactate Dehydrogenase
H&E	Hematoxylin and eosin stain
TUNEL	Transferase- mediated dUTP nick end-labeling
XTT	2,3-bis-(2-methoxy-4-nitro-5-sulfophenyl)-2H-tetrazolium-5-carboxanilide

Introduction

Metal-organic frameworks (MOFs), also known as porous coordination polymers, have been studied extensively for gas storage, catalysis, sensors, and membranes due to their high surface area/volume ratios and porosities¹. More recently, MOFs have also been investigated for drug delivery, beginning with loading and controlled release of ibuprofen^{2,3}. Subsequent applications of MOFs to drug delivery have still principally focused on the release of small molecule drugs, such as the antitumor agents doxorubicin and curcumin^{4–8}. A technique for encapsulating and protecting macromolecules using MOFs, termed biomimetic mineralization, has been used to generate MOFs loaded with a variety of macromolecular therapeutics (e.g. gelonin, Cas9 loaded with sgRNA for CRISPR, plasmids, and siRNAs)^{9–13}. Using MOFs to deliver therapeutics of all classes, including small molecules, gasotransmitters, proteins, nucleic acids, viruses, and cells is a growing area of investigation^{10,14–18}.

General reviews describing MOFs and their development are widely available ^{19,20}. Here, we will focus on the application of MOFs for drug delivery. Specifically, our goal is to describe methods and techniques used to generate and characterize MOFs for drug delivery applications. Syntheses and modifications of MOFs that are useful for enhancing their utility for drug delivery are explored. A variety of drug loading techniques specific to MOFs will be discussed. Cell culture and *in vivo* evaluation of MOF-drug formulations will also be highlighted to demonstrate progress to date in translating MOFs to clinical practice.

Structures and Compositions of MOFs

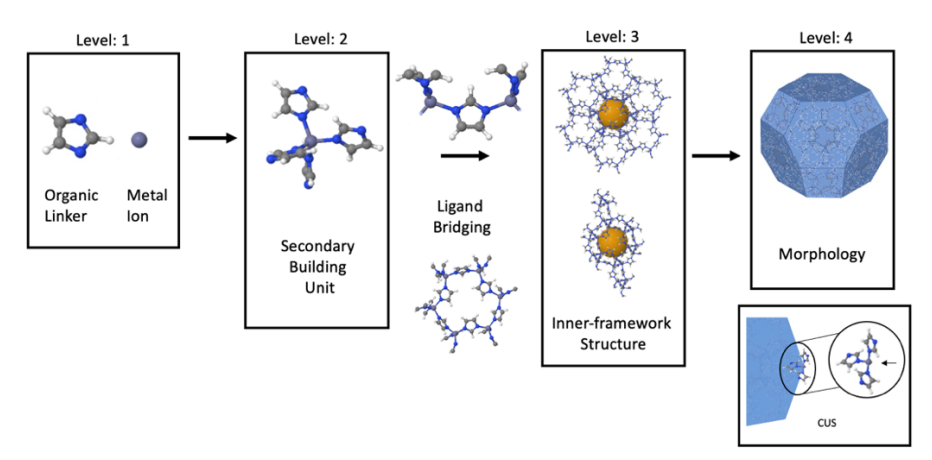


Figure 1: Levels of structure and composition for MOFs. Level 1 – node and linker; Level 2 – secondary building unit (SBU) and coordinatively unsaturated site (CUS); Level 3 – inner-framework structure, and Level 4 – morphology. Molecular models created with permission from ChemTube3D (http://www.ChemTube3D.com)

The structures of MOFs can be described on four levels (**Figure 1**). The first level is the chemical constituents used to construct the MOF, i.e., a metal ion (node) and a coordinating ligand (linker). Multivalent metal ions are most commonly used; however, monovalent ions have also been used²¹. Zirconium (IV), Iron (III), and Zinc (II) are the most prevalent ions used in MOFs intended for drug delivery applications (**Table 1**). The ligands used in MOF synthesis usually have multiple carboxyl or amine functional groups that extend from either an alkyl chain or a ring-based structure like benzene or imidazole. Coordination of the ligand with the ion results in a crystal-like lattice with regular repeating geometry. While most MOFs have rigid structures, others are known to demonstrate some structural flexibility^{22–24}.

The second level of structure is referred to as the secondary building unit (SBU), which is the coordination site of multiple ligands with a metal ion into a relatively rigid geometry²⁰. SBUs essentially serve as the template or unit cell for the growth of the MOF structure. The linking of multiple SBUs by bridging ligands, ligands linking two metal nodes, defines the internal framework, the third level of MOF structure. This third level encompasses the pores and cages (i.e., the void volume) of the MOF. The pore structure can generally be determined *a priori*, given a particular metal ion and ligand²⁰.

While the first three structural levels of MOFs are essentially predetermined by the coordinating metal and ligand²⁵, the outer morphology (size, shape, orientation), the fourth structural level of a MOF, depends on how the internal framework grows. The synthesis procedures used and whether molecules (e.g., therapeutics) are being encapsulated during synthesis will affect the outer morphology of the MOF^{7,9}. Also, MOFs contain coordinatively unsaturated metal sites (CUSs) that can act like Lewis acids and aid in loading molecules onto the surface and functionalizing the MOF^{6,25,26}. The fine, multilevel control of the chemical and structural features of MOFs makes them highly desirable for use in drug delivery applications.

Advantages for Drug Delivery

Though not originally developed with drug delivery in mind, MOFs have demonstrated their utility for drug delivery based on precise control over their size, structure, and pore dimensions; straightforward surface functionalization; high drug loading capacities; controlled release of therapeutics in biological environments; synergistic/dual drug loading/release; and protection/stabilization of biomolecular therapeutics. Synthetic methods can be altered to create nanosized MOFs or adjust the pore dimensions of the MOF to improve loading or control release^{27–30}. Additionally, modifications can be made synthetically or post synthetically that further improve loading, targeting, and the stability of MOFs in biological environments^{10,29,31–33}.

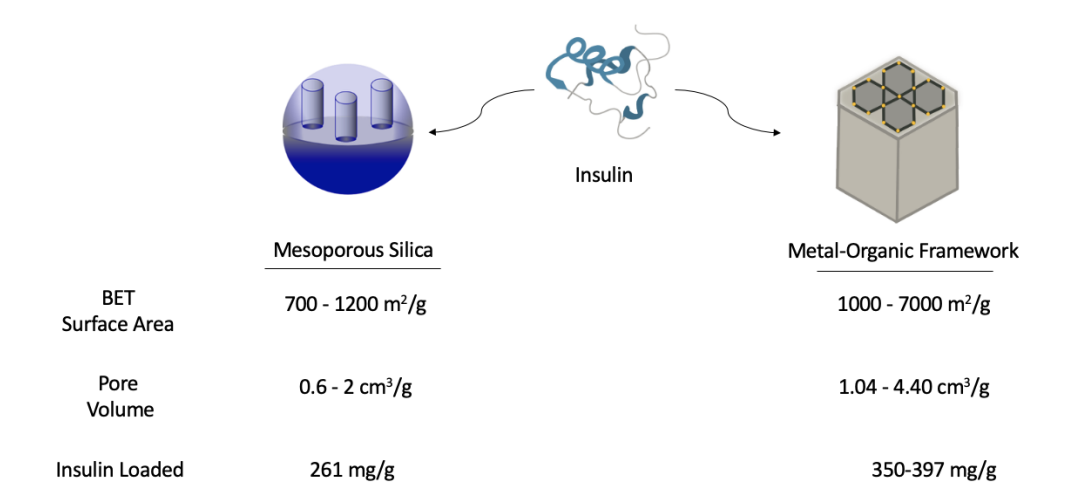


Figure 2: Surface area³⁴, pore volume³⁴, and insulin loading^{11,35} of MOFs in comparison to mesoporous silica³⁶. The large surface areas and pore volumes allow the higher drug loading achieved by MOFs.

With some of the most highly porous structures and largest surface areas reported for delivery vehicles³⁴, MOFs can load substantially more drug (e.g., **Figure 2**; insulin – mesoporous silica³⁶ (26.1 wt%) vs. MOF^{11,35} (35 - 39.7 wt%)), resulting in high local concentrations of drug when delivered from MOFs³⁷. Controlled release from MOFs has also been demonstrated^{38,39}. Release from some frameworks is inherently triggered by stimuli (pH, ATP, UV light, etc.)^{6,40–43}, and other frameworks are easily modified with moieties that control release of therapeutics from the pores^{44–49}. These stimuli triggered formulations have been reviewed⁵⁰. MOF pores can also be designed to slow or accelerate the diffusion of the therapeutic cargo^{4,22}. The rate of MOF degradation in biological environments, and hence the rate of drug release, can also be manipulated by choosing alternative chemical constituents^{4,22}. Depending on the loading method and MOF composition, synergistic therapeutic effects can be achieved either by loading multiple therapeutics in a single MOF or by the release of the metal or ligand from the MOF along with the therapeutic. This synergism has been proposed for cancer, vaccines, tendon healing, wound healing, and osteopathic applications^{14,40,51–56}.

MOFs can encapsulate a wide variety of small molecule and macromolecular therapeutics. They are particularly useful for encapsulating poorly water-soluble cancer therapeutics (e.g., curcumin) and gasotransmitter molecules (e.g., nitric oxide (NO), carbon monoxide (CO), and hydrogen sulfide (H₂S))^{6,18,55–57}. MOFs have also been shown to encapsulate macromolecular cargos (e.g., nucleic acids and proteins), stabilize their structures, and protect them from degradation in biological environments^{9,28}. Even larger cargos, like vaccines and cells have been explored (see Case Studies below)^{16,17,58}.

Synthesis and Characterization

The available chemical and physical properties space for MOFs is extensive, due to the number of possible ions and ligands (**Table 2**). Applying reticular chemistry (structure-guided synthesis) enables the design of MOF frameworks to suit the needs of a particular application and precludes exhaustive empirical investigations²⁰. Subsequent modifications can be made to the ligand while maintaining the overall geometry of the MOF framework (aka isoreticular chemistry). These modifications can be used to enact incremental changes in pore size, void volume, and surface area^{28,59–64}.

Controlling the structure and chemistry of the framework also controls the storage and release of the therapeutic molecules^{22,26–29,59}. In numerous cases, this control was gained by altering the charge of the framework^{26,59,65}. Multiple isoreticular MOF series have identified MOFs that are stable in biological fluids and have enhanced interactions with biomacromolecules³³. Functionalizing the ligand with an azide allowed for click chemistry⁶⁶, which was used in multiple studies to create stimuli responsive MOFs gated by DNA aptamers (oligonucleotides that bind a specific target through structural complementarity)^{44–49}.

In addition to these molecular-scale design options, the macroscopic size, morphology, and internal framework of the MOF can be controlled. Macroscopic order is achieved through controlled syntheses that use reaction kinetics, reagent/solvent ratios, equilibrium, temperature, and modulating agents to achieve the desired size and shape 33,55,67-69. Modulating agents, which are chemically similar to the MOF ligand, can act as competing ligands in the synthesis or deprotonating reagents that alter the nucleation and growth of the MOF^{29,68}. Furthermore, modulating agents can introduce defects into the MOF structure to achieve larger pore sizes or additional void space 7,29,65,70-73.

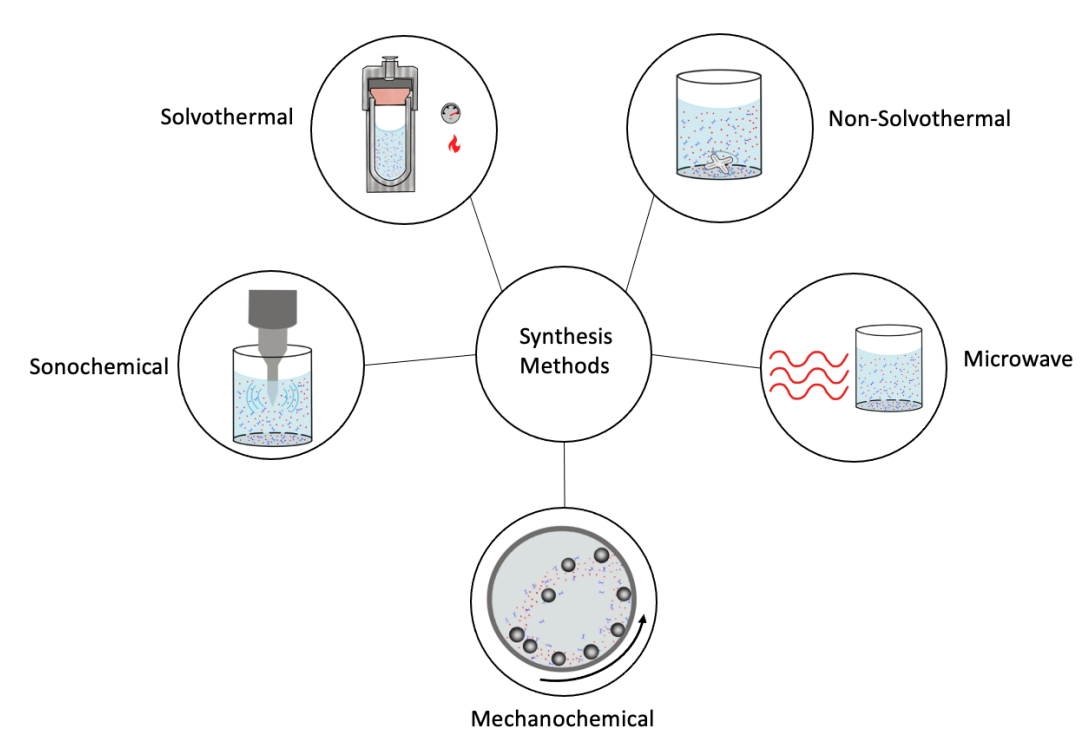


Figure 3: Methods of MOF synthesis. Solvothermal methods involve high temperatures and pressures, non-solvothermal methods do not⁷⁴. Microwaves can assist MOF syntheses⁷⁵. Mechanochemical methods use ball milling as a means of synthesis^{76–78}. Sonochemical methods use high-energy sonication to aid MOF formation^{29,79}.

A variety of synthesis methods allows for flexibility in MOF fabrication (**Figure 3**). Synthesis methods vary based on the MOF, with some MOFs synthesized by multiple methods⁷⁴ (**Table 2**). Solvothermal and non-solvothermal syntheses are commonly used for MOFs. Solvothermal synthesis is generally carried out above the boiling point or at high pressures to dissolve the reactants and promote synthesis. Non-solvothermal synthesis is carried out below the boiling point of the solvent and is generally carried out in reaction conditions that favor nucleation. Nontraditional synthesis methods used for drug delivery applications include microwaving⁷⁵, sonicating^{29,79}, or mechanical grinding^{76–78}. Many of these methods use organic solvents which can remain in the MOFs after synthesis and which can be subsequently removed by a process termed "activation"^{74,80}. To avoid solvent issues for biological applications, synthesis methods have been developed in aqueous conditions and using light alcohol solvents^{22,33,41,67,69}. Also, solvent-free, mechanical synthesis methods have been investigated^{76,78}.

After synthesis, MOFs are characterized by a variety of approaches. For example, a curcumin and zinc-based MOF, medi-MOF-1, was analyzed by powder X-ray diffraction (PXRD) to confirm its crystalline structure before and after exposure to different solvents⁵². As measured by thermogravimetric analysis (TGA), medi-MOF-1 maintained structural stability up to 300°C. Fourier Transform IR (FTIR) was used to confirm bonding and, later, ibuprofen loading⁵². Nitrogen adsorption was used to

determine the porous structure characteristics of medi-MOF-1, such as Brunauer-Emmett-Teller (BET) surface area (3002 m²/g) and pore volume (0.902 cm³/g) 52 . Molecular modeling was used to reveal the coordination scheme, confirm the SBU, pore diameters (9.2-11 Å), free volume (1.51 cm³/g), and simulated X-ray diffraction pattern of medi-MOF-1, while light-based microscopy was used to determine its size (~80-100 μ m) 52 . Scanning electron microscopy (SEM) and transmission electron microscopy (TEM) are also commonly used to visualize the macroscopic morphology of MOF particles, depending on their size 29,52 .

Tuning MOF Characteristics for Drug Delivery

Post-synthetic functionalization and modification of MOFs can be used to improve drug loading and release kinetics and control their behaviors in biological environments. MOFs can be modified to improve loading by adding moieties that provide favorable interactions for loading. For instance, cationic polymers, like poly ethyleneimine (PEI) and ethanolamine conjugated poly(glycidyl methacrylate) (PGME(EA)), have been added to the synthesis or attached post-synthetically to increase the loading of polyanionic nucleic acids^{15,81}. Post-synthetic functionalization of the ligand to introduce a positive charge improved loading of the anionic anti-inflammatory drug diclofenac⁵⁹. Similar ligand modifications have allowed for gasotransmitter storage^{55,56}.

In addition to modifications that improve loading, modifications can be made to control release. Biomineralization of Ca₃(PO₄)₂ on the surface of a MOF limited the release of CpG oligonucleotides (immunostimulatory DNA sequences containing repeats of cytosine (C) followed by guanine (G)). When exposed to acidic environments, the calcium phosphate coating degraded and phosphate ions were liberated, triggering the release of CpG oligonucleotides from the surface of the MOF and inducing an immune response⁶⁵. DNA-aptamer gated MOFs were created by using click chemistry to attach DNA to the surface of a MOF^{44–49}. The DNA-aptamer blocked the release of drugs from the MOF until triggered by binding to its target. Similarly, addition of an amino group to a MOF ligand allowed attachment of a cytosine rich DNA, enabling the pH-triggered release of rhodamine⁸². A reactive oxygen species (ROS) responsive polymer coating provided light responsive drug release and stabilization in biological environments³⁷. MOF entrapment in a hydrophobic polymer scaffold permitted the prolonged release of NO^{55,56}.

Coatings, ranging from polymers and biomolecules to entire cell membranes^{8,10,31,54,75}, have been added to MOFs to improve targeting, colloidal stability, and biological half-life. Platelet membrane coated MOFs selectively delivered siRNAs to cancer cells in an *in vivo* mouse model³¹. MDA-MB-231 extracellular vesicle (EV) membrane coated MOFs showed homotypic uptake targeting to MDA-MB-231 cells and

also were preferentially endocytosed by tumor cells *in vivo*¹⁰. In both cases, membrane coatings also improved the colloidal stability and solubility of the MOF. Coating with CpG oligonucleotides stimulated an immune response *in vivo* and improved solubility⁸³. Coating with albumin improved biorecognition, colloidal stability, and cell adsorption while reducing toxicity⁸⁴. Chitosan and polyvinylpyrrolidone (PVP) coatings increased colloidal stability and biocompatibility^{32,79}. Similarly, a capping of cetyltrimethylammonium bromide (CTAB), a surfactant, was used to maintain dispersity in suspension⁸⁵. Methoxy poly(ethylene glycol)-block-poly(L-lactide) polymers were used to protect MOF-drug complexes for oral delivery of insulin from acidic degradation in the stomach (see Case Studies below)¹¹. MOF-polymer nanocomposites have been comprehensively reviewed elsewhere⁸⁶.

Mechanical and thermal modifications have also been applied in the manipulation of MOF structures. Ball milling and mechanical grinding have been used to decrease MOF size to take advantage of the enhanced permeability and retention (EPR) effect in cancer or to increase biocompatibility^{87,88}. In one case, ball milling was used to create unsaturated Zn and N-sites on a MOF surface, which allowed for water binding and improved biocompatibility⁸⁸. Mechanical grinding was used to control release kinetics by amorphizing the MOF and, potentially, blocking pore openings^{38,39}. Similarly, thermal treatment, leading to partial pore collapse, was used to slow and extend drug release profiles⁸⁹.

Drug Loading, Encapsulation, and Release

MOFs are attractive as drug delivery vehicles principally due to their exceptional drug loading capacity. Drug loading is governed by the physical properties of the MOF (i.e., pore size, surface area, void volume, and structural dynamics)². Variable sized pores and void volumes can be exploited for loading multiple therapeutics. Sequential loading in order of drug size (largest first) enables multiple drugs to be loaded into a single structure. For example, catalase (4.9 x 4.4 x 5.6 nm) was loaded into a MOF to fill 5.5 nm pores, followed by loading of superoxide dismutase (2.9 x 3.5 x 4.2 nm) to fill 4.2 nm pores. This structure with the combined antioxidant activity of the two enzymes effectively reduced ROS accumulation in stressed cells⁷⁰.

MOF pores may be rigid or more flexible, depending on the composition of the MOF and guest-host interactions²². MOF pores exhibit breathing, swelling, ligand rotations, and subnetwork displacements^{23,90}. MOF breathing, in which unit cell structures change upon binding to the loaded molecules, has been associated with loading and release of host molecules, like ibuprofen²⁷ and NO²⁴. Swelling, where the unit cell expands while maintaining its shape, is also dependent on guest-host interactions and has been associated with release of ibuprofen^{90,91}. Ligand rotation occurs around the metal coordination centers, which allows for expansion of the pore

opening⁹². Subnetwork displacements can occur when connecting forces are relatively weak and allow the relocation, drifting, and shifting of MOF components²³. To make use of these dynamics, efforts have been made to understand which SBUs, ligands, and metal ions allow dynamic flexibility in the structure of the MOF²³. While ligand rotation and subnetwork displacements have not been explored in drug loading and release, they have in gas storage and may explain some release phenomena⁹⁰.

Chemical properties further govern the stabilization and loading of therapeutics on or within MOFs. Therapeutic molecules and MOFs can interact through van der Waals forces or specific molecular features of the MOF, such as through Watson Crick base pairing with nucleic acid-based MOFs of the MOF, such as through Watson Crick base pairing with nucleic acid-based MOFs of the MOF, such as through Watson Crick base pairing with nucleic acid-based MOFs of the MOF, such as through Watson Crick base pairing with nucleic acid-based MOFs of the MOF, such as through Watson Crick base pairing with nucleic acid-based MOFs of the MOF, such as through Watson Crick base pairing with nucleic acid-based MOFs of the MOF, such as through Watson Crick base pairing with nucleic acid-based many MOF ligands contribute to favorable π - π stacking interactions in loading molecules such as 5-fluorouracil 93 , mitoxantrone 33 , rhodamine 73 , and doxorubicin 5 . CUSs participate in surface coordination interactions with therapeutics such as nucleic acids (phosphatemetal) 26,65,94,95 and small drug molecules like curcumin and doxorubicin 5,6 . CUSs are also critical in the loading and release of gasotransmitters; in some cases, CUSs can form chelating bridges with these gaseous therapeutics 96 . Electrostatic forces governed the loading of siRNAs and diclofenac 26,59 . Other small molecule drugs like oridonin leveraged hydrogen bonding to enhance loading 97 . As pH affects electrostatic interactions and hydrogen bonding, the pH during loading and the pH of the desired release environment should be considered when optimizing drug loading.

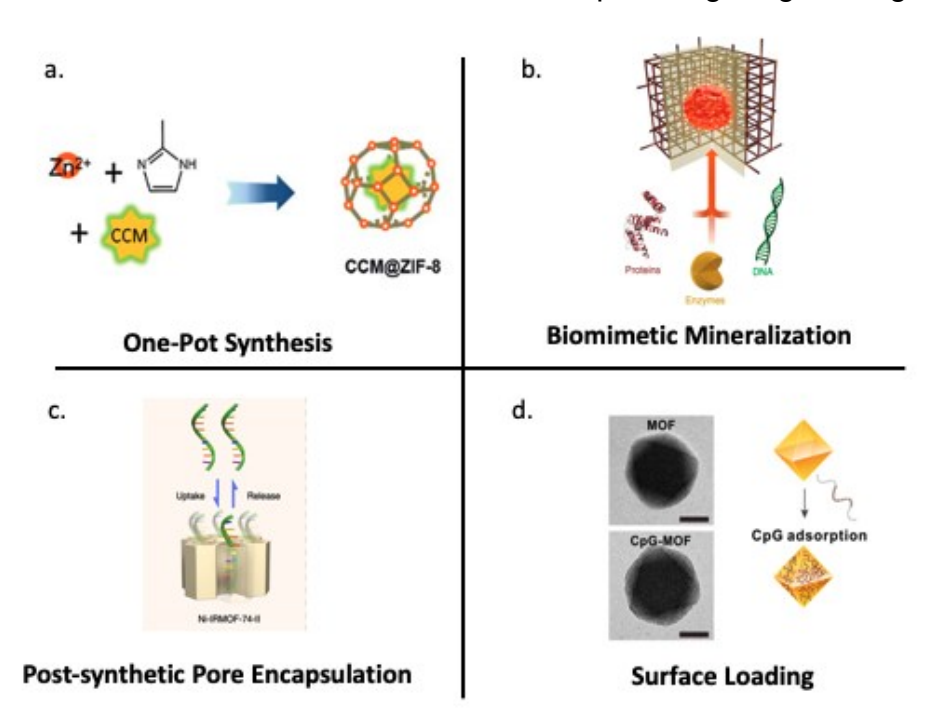


Figure 4: Loading and encapsulation methods. **(a)** One-Pot synthesis⁸, **(b)** biomimetic mineralization⁹, **(c)** post-synthetic pore encapsulation²⁸ and **(d)** surface loading⁶⁵. Reproduced with permission from ref 8, [2018, The Royal Society of Chemistry], ref 9, [2015, Springer Nature], and ref 28, [2018, Springer Nature].

Loading method is critical for maximizing loading and achieving desired release profiles. There are four common methods for loading MOFs with drugs: one-pot synthesis, biomimetic mineralization, post-synthetic encapsulation, and surface loading (**Figure 4**). One-pot syntheses involve the coprecipitation of the therapeutic molecule with the MOF during synthesis. This leads to relatively uniform distribution of drug molecules throughout the mesopores of the MOF⁴. To avoid degradation of the therapeutic by the solvents used in most one-pot approaches, a mechanical one-pot synthesis method was developed, though its application has been limited to small molecule therapeutics^{76,77}. One-pot synthesis is convenient for protecting the therapeutic and usually degradation of the MOF controls release, provided the pore sizes are sufficiently small to limit rapid diffusion of the drug from the MOF structure^{83,85}.

Biomimetic mineralization is useful for loading of biomolecular therapeutics like proteins and nucleic acids. Similar to one-pot synthesis, biomimetic mineralization combines biomolecules and MOF base units in one reaction mixture. Distinct from one-pot synthesis, biomimetic mineralization relies on the biomolecule as a nucleation site for MOF crystallization^{9,98}. Specifically, biomolecular moieties form favorable bonds/interactions with MOF building units thus facilitating nucleation. The biomolecule being encapsulated thereby determines the size, morphology, and crystallinity of the MOF, while simultaneously being encapsulated in a MOF shell. This encapsulation mechanism has been shown to protect biomolecules from harsh chemical environments, heat, and degrading enzymes⁹. Due to integration of the therapeutic into the MOF structure, its release relies on the degradation of the MOF, which can result in 'slow' release and delayed activity of the encapsulated therapeutic^{15,16,99,100}.

Post-synthetic encapsulation involves the loading of therapeutic molecules inside the pores of the MOF after synthesis. This is typically achieved by mixing the MOF and therapeutic in a solvent followed by removal of the solvent via evaporation 11,28,101. Excess therapeutic is then washed from the surface. Alternatively, sonication and mechanical grinding have also been used for post-synthetic encapsulation 33,37,87. For gasotransmitter loading, gravimetric adsorption is used 24,96,102. Post-synthetic encapsulation generally results in diffusive release that can be accelerated by degradation of the MOF or by changes in environmental factors like pH^{22,27,52,59}. Alternatively, MOFs with smaller pore sizes have demonstrated only burst release associated with their degradation (i.e., no diffusion through pores; rapid release due to MOF degradation over a short time period)^{22,52}.

Surface loading is generally governed by CUS interactions and electrostatic interactions but can depend on other interactions^{5,83,85,94,95,103,104}. Surface loading can also be achieved by linking the therapeutic to the surface of a polymer coating¹⁰⁴. Surface loading often results in reduced drug loading compared to other methods and rapid release of the drug from the MOF^{4,5,8,81,85}. For example, surface loading led to 4.9

wt% doxorubicin loading⁵ vs. 14-20 wt% for one-pot loading⁴ in ZIF-8 (Zeolitic-imidazole framework-8 composed of Zn²⁺ and 2-methlyimidazole). Interestingly, in this case, surface loading was not accompanied by rapid drug release, as doxorubicin complexes strongly and preferentially to the surface of ZIF-8. Surface loading is particularly useful for loading additional therapeutics onto a MOF already loaded with encapsulated therapeutic⁹⁵. In general, regardless of the encapsulation approach, MOFs protect biomolecules from degradation and expand the potential routes that could be used for clinical administration. That said, proteins/enzymes may change conformation when adsorbed to the MOFs surface¹⁰⁵.

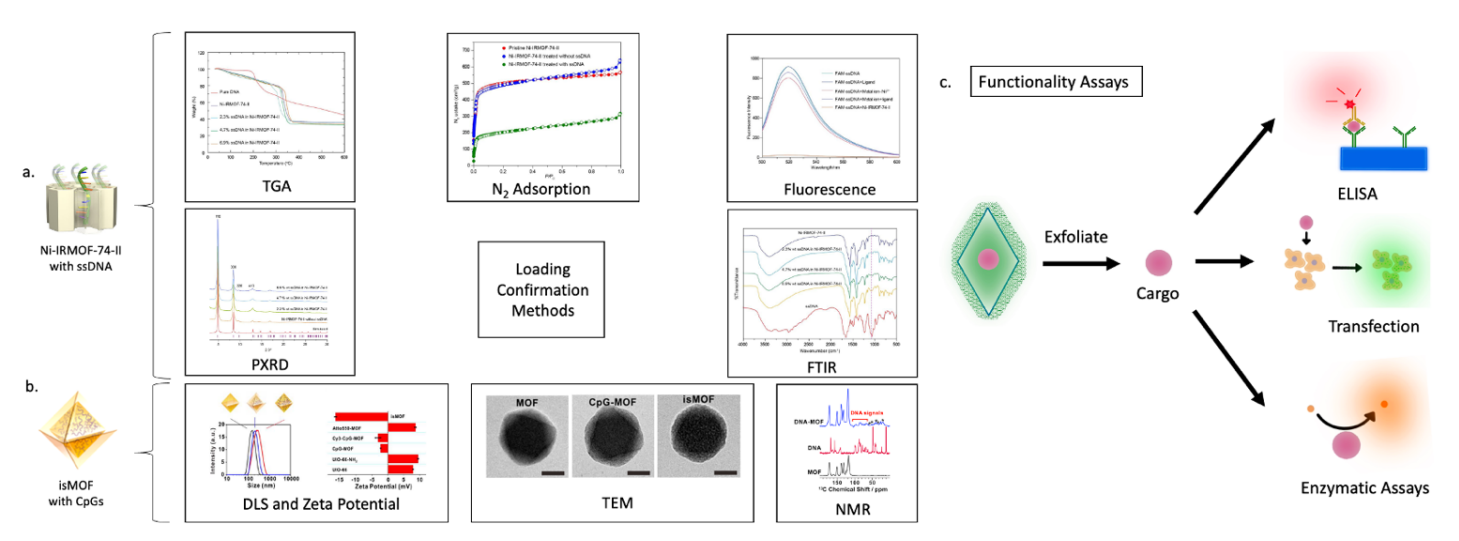


Figure 5: Methods to confirm drug loading and function. **(a)** Methods used to characterize Ni-IRMOF-74-II loading with ssDNA²⁸ **(b)** Methods used to characterize isMOF (UiO-66 surface loaded with CpGs and coated with Ca₃(PO₄)₂⁶⁵, **(c)** Functional assays to confirm macromolecular therapeutic function after loading and release from MOFs. Reproduced with permission from ref 28. [2018, Springer Nature].

Drug loading is often confirmed using TGA^{5,6,28,33,52,87}. Protection of the drug from degradation can also be assessed by TGA^{6,106}. Reduction in the available surface area and pore volume (e.g., as measured by nitrogen adsorption-desorption) has been used to confirm loading^{27,95}. TEM can be used to confirm mesopores formed by incorporating therapeutics in the structure of the MOF or morphology/size changes^{4,65}. Fluorescence measurements have also been used to confirm loading for Calcein and biomolecules with fluorescent tags^{28,29,35,75}. For surface loaded therapeutics, measuring the zeta potential and size of the MOF after loading serves as a way to determine the presence of the drug^{65,107}. FTIR, NMR, and PXRD are also applied to confirm the fidelity of MOF synthesis and drug loading/encapsulation simultaneously (**Figure 5a and 5b**)^{6,9,59,108}. To confirm drug activity after loading, principally for macromolecular therapeutics, functional assays such as enzyme-linked immunosorbent assays (ELISAs)^{16,35},

enzymatic assays^{9,70}, and transfections⁹⁹ have been performed after release of the therapeutic from the MOF (**Figure 5c**).

ssDNA loading into Ni-IRMOF-74-X was confirmed by shifts in the TGA curves relative to the unloaded Ni-IRMOF-74 MOF (**Figure 5a**)²⁸. Nitrogen adsorption analysis showed that pore volume had decreased from 0.78 to 0.45 cm³/g due to ssDNA loading. The appearance of an FTIR peak at 1050 cm⁻¹ confirmed ssDNA incorporation, a conclusion reinforced by quenching of the fluorescence probe on the ssDNA. Lastly, PXRD analysis showed additional peaks appearing after ssDNA loading²⁸. Dynamic light scattering and zeta potential were used to measure loading of CpGs (negatively charged) onto isMOF (**Figure 5b**)⁶⁵. Morphology changes and size changes, determined by TEM, further confirmed surface loading of CpGs. The appearance of peaks related to DNA in the NMR spectrum further confirmed CpG loading⁶⁵.

Biocompatibility, Cellular Targeting, and Uptake

To be useful as clinical drug delivery vehicles, MOFs have to be biocompatible with limited cytotoxicity and immunogenicity. The cytotoxicity of MOFs is complicated by the fact that any of the components can be toxic alone but not when structured in the MOF and vice versa^{10,89,109}. Moreover, cytotoxicity has also been shown to be cell type dependent¹¹⁰. The metal ions and ligand alone need to be biocompatible as each can leach into the biological fluid/tissue over time^{33,35,111}. In fact, toxicity of the same MOF depended on the metal ion (Fe vs. Cr)¹¹⁰. The most widely used MOF in biological applications, ZIF-8 (**Table 1**), was evaluated in laboratory buffers for structural changes and leakines¹⁰⁰. Structural changes were common with most buffers, but leakiness was only an issue with cell medium, serum, and 0.1 M bicarbonate solutions. In cytotoxicity studies, ZIF-8 was well tolerated up to 100 µg/mL in cell culture 109, with similar biocompatibility seen for the related MOF, ZIF-90⁴¹. MIL(Fe) MOFs were tolerated up to 2 mg/mL in cell culture¹⁰⁹. The difference in toxicity between ZIF and MIL(Fe) MOFs (**Table 3**) was hypothesized to be due to Zn²⁺ competition with Fe²⁺ and Ca²⁺ for ion channels and/or DNA damage caused by excess Zn^{2+ 109}. Zirconium based MOFs showed a broad range of biocompatibilities (50 µg/mL - 1.6 mg/mL)^{37,89,109}. A gadolinium-based MOF was biocompatible to 300 µg/mL in a mouse model; minimal Gd³⁺ leaching was reported in mimicked biological fluid (450 parts per billion)⁸⁷, mitigating concerns about Gd³⁺ toxicity (associated with cell iron transport) which can occur at ppm concentrations^{112,113}.

In general, immune stimulation from drugs is undesired as it leads to increased clearance rates and inflammation^{73,114}. Mixed results have been reported in regard to the immunogenicity of MOFs. Some studies find uncoated MOFs initiate no significant immune response compared to untreated cells^{73,115} while other studies showed that coated MOF systems (by EVs¹⁰, by chitosan¹¹⁵, or by heparin^{103,116}) were less

immunostimulatory than uncoated MOFs. Note, these findings depended on the immune response inspected (e.g., macrophage internalization and expression 10,73,103,116, Th1 immune response 104,107,115,116, or complement system response 115,116). For some therapeutic applications (e.g., subunit vaccines), immunogenicity of the delivery vehicle is an advantage 40,65,83,104. In subunit vaccine applications, CpG coatings are commonly included for immune activation 40,65,83,104. Continued study of immunogenicity will be necessary in the development of clinical MOF formulations.

For clinical application, MOFs need to maintain their structure, dispersion, and chemical functionality in biological fluids, which has been achieved by some MOFs^{29,30,33,35,117} but not others^{79,88}. Ligand functional groups and surface charge (as measured by zeta potential) can determine colloidal stability of the MOFs in biological fluids^{26,33}. Formation of a protein corona improved the colloidal stability of MOFs^{26,33,38,84} and their cellular uptake⁸⁴. Membrane coatings also improved colloidal stability^{10,31,75}. PVP, chitosan, polyethylene glycol (PEG), hydrogels, and 1,2-dioleoylsn-glycero-3-phosphocholine (DOPC) have all been used as coatings to prevent aggregation^{11,32,37,47,79,110}. Even nucleic acids loaded onto the surface of a MOF have been shown to increase colloidal stability^{51,83}.

Limiting systemic toxicity is an important consideration for drug development. One approach to targeting MOF-based drugs to only the diseased cells is through surface functionalization with a targeting moiety or coating. Functionalization of a MOF surface can be achieved readily by reacting primary amines found on MOF ligands ¹¹⁸. MOFs have been functionalized with folic acid ^{119,120}, HER2/Neu antibody ¹²¹, RGD-peptide ¹²², hyaluronic acid ^{8,123}, and AS1411 aptamer ^{48,49,124} or coated with cellular membrane materials ^{10,31} for targeting cancer cells. A MOF was functionalized with MK6240, a tau positron emission tomography tracer, to target neurofibrillary tangles for the diagnosis and treatment of Alzheimer's disease ¹²⁵. Novel passive targeting strategies have also been used. Temporal, *in vivo* aggregation of MIL-100 allowed for passive targeting of lungs ¹²⁶. Successful targeting methods will be important for reducing systemic toxicity and translation of MOFs to clinical applications.

In vivo studies have shown MOF delivery systems to be well tolerated with and without modifications. In many cases, *in vivo* biocompatibility was achieved despite observed cytotoxicity in cell culture¹⁰, perhaps due to the formation of a protein corona *in vivo*^{33,84,111}. ZIF-8 delivery systems without modifications showed no significant toxicity or pathology and achieved good therapeutic outcomes^{10,16}. Additionally, Gd-pDBI, ZrDTBA, UiO-66, MIL-100 (Fe), HUSKT-1, and porphyrin based MOFs have all been tested *in vivo* without evidence of toxicity^{6,37,73,87,119,126}. Similarly, coated MOFs were also biocompatible when delivered subcutaneously, intravenously, or orally and also demonstrated desired therapeutic effects^{10,11,16,37,40,55,56,83,120,122,124,125,127}.

Because some therapeutics, like siRNAs, need to be internalized by cells to achieve a therapeutic effect, cellular uptake of MOF-drug complexes has been

investigated^{10,11,41,54,65,108}. To date, few generalizations can be made about endocytosis of MOF-drug complexes. MOF endocytosis has been shown to be energy dependent^{54,128}. Furthermore, MOF size, coatings, and surface charge affect the mechanism of endocytosis^{65,89,128}. MOF size has a significant effect on uptake, with one study finding 90 nm to be optimal²⁹. Surface modifications, such as addition of bioactive agents like CpG oligonucleotides or targeting moieties like triphenyl phosphonium ions, can improve intracellular accumulation^{65,108}. NU-1000 (a Zr⁴⁺ and 1,3,6,8-tetrakis(p-benzoate) pyrene-based MOF) has been shown to primarily use caveolae mediated endocytosis in HeLa cells⁸⁹. However, it is likely that the route of endocytosis will vary by cell type and influence the efficacy of the delivered carg¹²⁹.

Endosomal escape is critical for function of delivered therapeutics³⁰. As with uptake, endosomal escape of MOFs depends on the MOF chemistry, structure, and modifications. Endosomal escape has been attributed to the "proton sponge effect"^{10,12,31,32}, where endosomal acidification results in swelling and rupture, and metal-ion mediated disruption of phosphate groups in endosomal membranes^{51,95}. Other MOF systems require the assistance of other molecules to aid their endosomal escape (e.g., NU-1000 based delivery of siRNA required NH₄CL and KALA peptide)^{30,108}.

Case Studies

This section showcases the unique capabilities MOFs offer for drug delivery. Specifically, the precision structural tuning of MOFs, the biomolecular and cellular protection MOFs offer, and their application to gasotransmitter release and catalytic nanomedicine will be discussed. Information on other MOFs and their delivery applications have been tabulated (**Table 1**).

Fine Control of MOF Pore Dimensions for Delivery of Specific Therapeutic Cargos

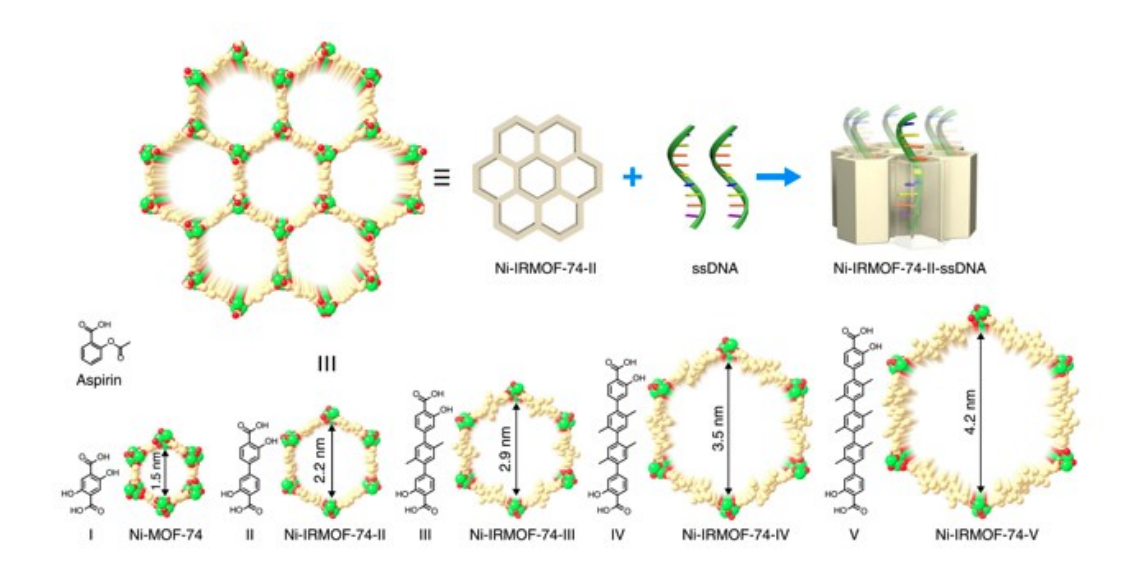


Figure 6: MOF ligand expansion used to increase pore size and tailor the loading of ssDNA²⁸. Reproduced with permission from ref 28. [2018, Springer Nature].

The pore structures of MOFs can be finely tuned to accommodate specific therapeutic cargos as described by Peng and colleagues²⁸. This group generated an isoreticular series of Ni-MOF-74 by extending its salicylic acid ligand with phenylene units, which created the tailored porosity and pore size needed to encapsulate and control the release of ssDNA (**Figure 6**). Specifically, Ni-IRMOF-74-II (pore size 2.2 nm) was found to precisely control ssDNA incorporation (governed by Van der Waals interactions) and release (triggered by the presence of complementary DNA). Ni-IRMOF-74-II protected ssDNA from nucleases in 10% fetal bovine serum and achieved a loading of 6.9 wt% (as compared to commercial lipid reagents LipoGene 2000 (0.02%) and Neofect (0.1%)). This formulation matched or bettered commercial reagents for transfection of macrophages, breast cancer cells, and CD4+ T cells and B cells while causing significantly less cell death. This study comprehensively showed the promise MOFs offer transfecting conventionally difficult to transfect cell lines and showcases the precision tuning of MOFs for precise control of loading and release of large biomolecules²⁸.

MOFs for Oral Delivery of Protein Therapeutics

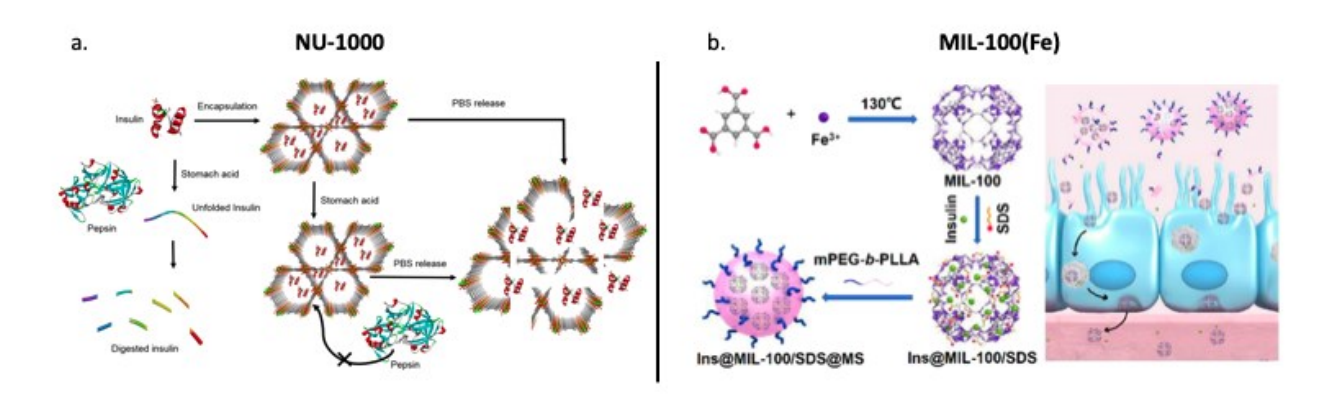


Figure 7: MOF formulations for oral insulin delivery. (a) NU-1000 system³⁵; (b) MIL-100(Fe) formulation¹¹.

Oral administration of therapeutics remains the most straightforward approach for maximizing patient compliance. Barriers to oral protein delivery include the gastrointestinal environment (acidic and proteolytic enzymes) and low permeability of protein drugs across biological membranes in the intestines¹³⁰. Two studies have investigated MOFs as a solution for oral delivery of protein therapeutics, specifically insulin. Chen et al. developed a Zr-based MOF (NU-1000) insulin delivery system (**Figure 7a**), which is acid resistant, has pores that favorably interact with insulin, and disassembles in the presence of phosphate ions (as in blood). NU-1000 was able to load 39.7 wt% insulin via post-synthetic pore encapsulation. Insulin loaded NU-1000 was stable in a simulated gastrointestinal environment and readily released insulin at physiological conditions (pH 7.0 in PBS)³⁵.

A polymer microsphere system was developed that successively encapsulated insulin and SDS in MIL-100¹¹ (**Figure 7b**). The methoxy poly (ethylene glycol)-block-poly(L-lactide) polymer coating protected the MOF from degrading in the gastrointestinal environment, and the SDS increased the permeability through the intestinal membrane. In monolayer, Caco-2 cell culture, the MIL-100 NP increased endocytosis of insulin and demonstrated good permeability of the monolayer. In a BALB/c mouse, type I diabetes model, this oral delivery system, at 50 IU/kg, reached a maximum plasma insulin level (~50 mIU/mL) at 4 h and remained elevated for 8 h. This system reduced glucose levels more slowly and for longer than subcutaneous injections. Furthermore, insulin accumulation in the liver suggested that insulin released from the MOF circulated through the portal veins to the liver and subsequently the cardiac tissue, closely mimicking endogenous insulin circulation patterns¹¹.

MOFs for Long-Term, Ambient Storage of Viruses and Cells

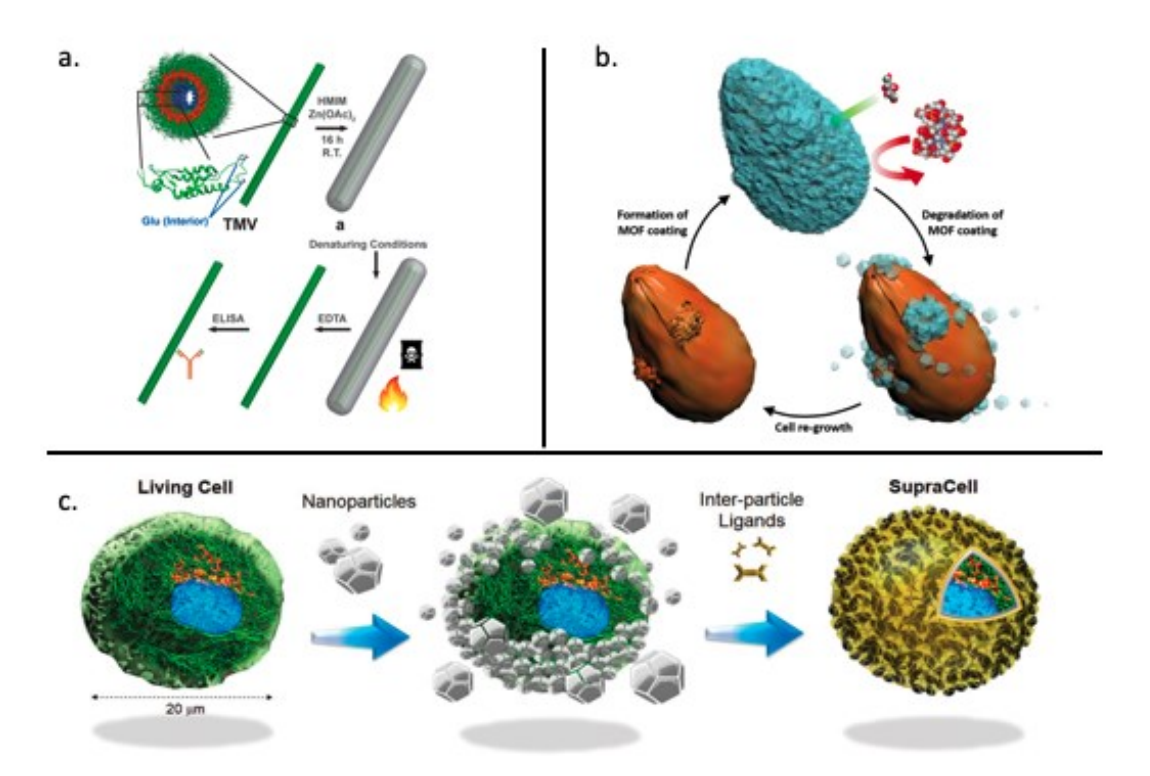


Figure 8: Biomimetic mineralization for the encapsulation and delivery of **(a)** TMV¹⁶ and **(b)** cytoprotective exoskeletons¹⁷ for living cells. **(c)** SupraCell construction for encapsulating living cells⁵⁸. Reproduced with permission from ref 17, [2016, John Wiley and Sons] and ref 58, [2019, John Wiley and Sons].

Recent work by the Gassensmith group has explored the enhanced stability and controlled delivery of a MOF-encapsulated tobacco mosaic virus (TMV). Interestingly, their controlled biomimetic mineralization process created a rod-shaped nanocoating over TMV^{98,131} (**Figure 8a**). This coating was put under the stress of protein destabilizing agents (methanol, ethyl acetate, 6 M guanidinium chloride) and heat (100°C) and was found to maintain the structure of TMV as determined by ELISA. The vaccine@MOF formulation was further demonstrated to elicit an antibody response in Balb/C mice comparable to the naked TMV, with no apparent toxicity¹⁶. This study demonstrates the possibility of MOF-based vaccine formulations that are stable without refrigeration, alleviating the significant cold-chain requirements of current vaccine formulations¹³² (including mRNA-based COVID-19 vaccine formulations).

An emerging application of MOFs involves their use in creating cytoprotective, diffusion controlling exoskeletons. A ZIF-8 coating on *Saccharomyces cerevisiae* (baker's yeast) was shown by Liang and colleagues to control molecular trafficking to the cell and prevent division, inducing an artificial hibernation state¹⁷ (**Figure 8b**). Upon exfoliation of the ZIF-8 exoskeleton, the yeast regained full function. Furthermore,

studies have encapsulated mammalian cells in MOF-based exoskeletons named SupraCells (**Figure 8c**). These coatings have been generated using ZIF-8, MIL-100, and UiO-66 MOFs and tannic acid. The exoskeleton coatings cause a quiescent cell state preventing replication or adherence to surfaces and conferring resistance to extreme environmental conditions. Exoskeleton coated cells were shown to resist osmotic stress, ROS, pH, and UV exposure and return to normal activities after exfoliation⁵⁸. One clear application for these coated cells would be delivery of probiotic bacterial supplements for gut health.

MOF-based Gasotransmitter Delivery

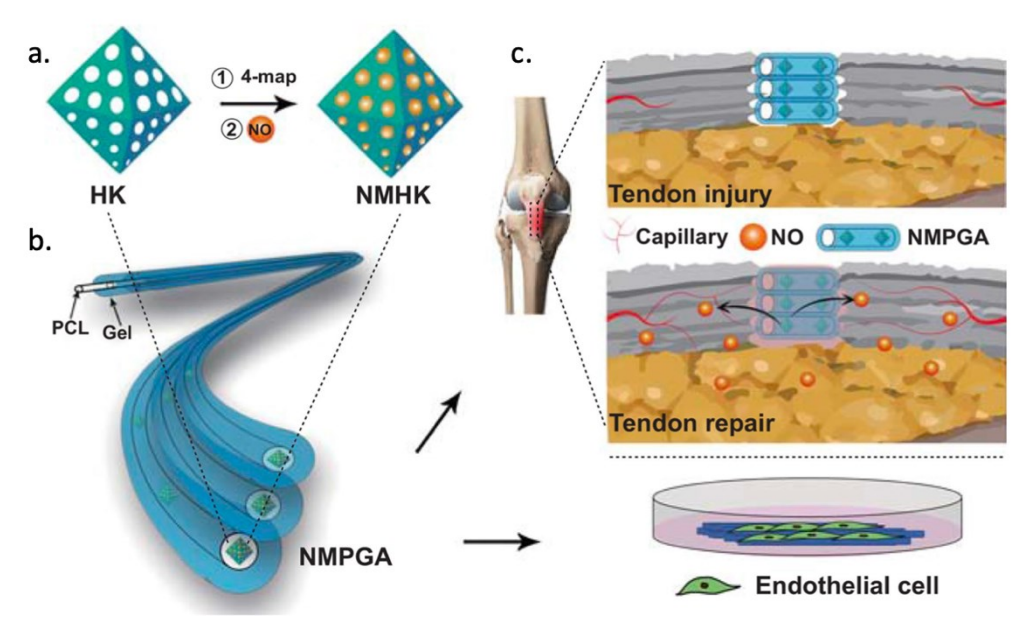


Figure 9: MOF-based nitric oxide (NO) delivery⁵⁶. **(a)** HKUST-1(HK) after post-synthetic modification with 4-methylamino pyridine and loading of NO becomes NMHK. **(b)** HK is embedded in a polycaprolactone (PCL)/gelatin (Gel) scaffold to generate NMPGA. **(c)** The scaffold material was applied to an *in vivo* tendon defect model and a cultured endothelial cell model. Reproduced with permission from ref 56. [2020, Springer Nature].

NO, CO, and H₂S are gaseous signaling molecules that are endogenously generated, freely traverse cellular environments, and play important roles in normal physiological processes¹³³. Because their balance in physiological processes is so delicate, their delivery as a therapeutic has been difficult¹⁸. MOFs have been identified as excellent candidates for controlled gasotransmitter delivery²², and applications have since been pursued and reviewed^{18,55,56,96,102}.

In one case, a copper MOF-based NO delivery system was developed to support tendon regeneration (**Figure 9**)⁵⁶. NO was encapsulated in the MOF (HKUST-1), which was further embedded in a hydrophobic polycaprolactone/gelatin scaffold to control water triggered NO release. This system sustained controlled release of NO over 15 days at 1.67 nM h⁻¹ while simultaneously releasing Cu²⁺ from the degrading MOF. The combined NO and Cu²⁺ release synergistically supported angiogenesis and collagen formation. This system supported tendon healing *in vivo* over a period of 70 days. A similar system was also applied to diabetic wound healing⁵⁵. These examples notwithstanding, gasotransmitter delivery represents a small portion of the MOF-based therapeutic literature and will require considerably more study for translation to clinical application¹⁸.

Catalytic MOF-based Nanomedicine

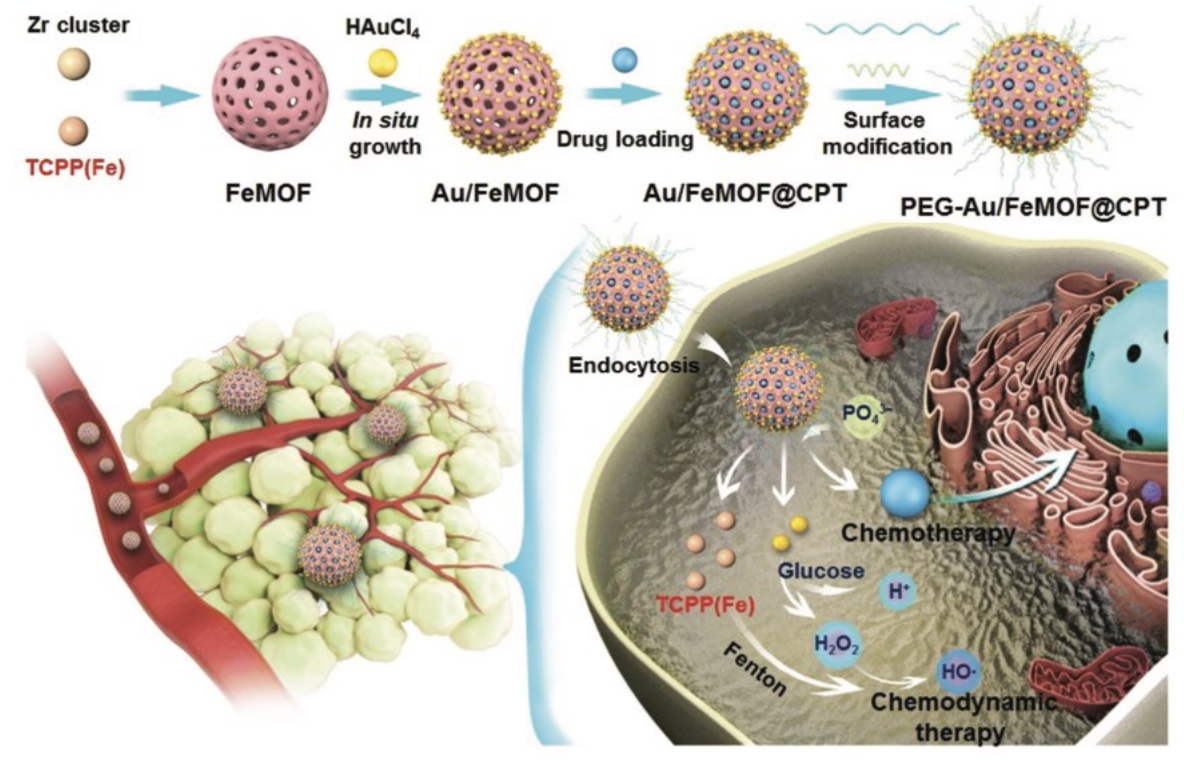


Figure 10: Catalytic MOF-based cancer therapy – synthesis (top) and mechanism of action (bottom)⁵⁴. Reproduced with permission from ref 54. [2020, John Wiley and Sons].

Catalytic nanomedicine is a unique and growing application of MOFs, as they are able to act as catalysts themselves or provide a scaffold for other catalytic species. Prior reviews have covered MOF-based catalytic nanomedicine applications in tumor therapies, bacterial disinfection, tissue regeneration, and biosensors^{134–136}. Cancerbased applications represent the bulk of the catalytic nanomedicine literature. MOF-based catalytic nanomedicine therapies take advantage of the tumor microenvironment (acidosis, high-glucose conditions, hydrogen peroxide, lactate, and glutathione overproduction) to initiate a series of cytotoxic chemical reactions^{54,119,127,136–141}.

One zirconium and iron (III) meso-tetra(4-carboxyphenyl) porphine chloride (TCPP(Fe)) MOF was used as a scaffold for gold nanoparticles (AuNP) while also being loaded with the chemotherapeutic drug camptothecin (CPT). The loaded MOFs were then coated with PEG (top of **Figure 10**)⁵⁴. These nanoMOFs (nMOFs), when delivered intravenously in mice, exploited the EPR effect as a means of passively targeting a xenograft tumor. Once present in the tumor environment, the nMOF scaffold degraded quickly in the presence of phosphate ions, thereby releasing the TCPP(Fe) ligand, AuNPs, and CPT and initiating a catalytic cascade. The released AuNPs functioned as a glucose oxidase mimicking catalyst, breaking down glucose into gluconic acid and

hydrogen peroxide. The TCPP(Fe) ligand reacted with the hydrogen peroxide in a Fenton type reaction generating cytotoxic hydroxyl radicals (**Figure 10**, bottom). nMOFs significantly inhibited tumor growth (85.6% inhibition of growth compared to an untreated control) over the course of 20 days⁵⁴. MOF-based, catalytic nanomedicine is an emerging application of MOFs with great promise to reduce the cost of drug development, reduce systemic toxicity, and overcome drug resistance¹³⁶.

Conclusions and Future Perspectives

MOFs hold great promise for the delivery of biomacromolecular and cellular therapeutics. It is straightforward to envision using MOFs as a component of a delivery system that specifically serves the purpose of loading and protecting biomolecules/cells. Then, post-loading modifications, like polymeric nanoparticle encapsulation or membrane coating, would be used to formulate the final therapeutic. These types of composite vehicle approaches are beginning to show promise *in vivo*^{10,11}. Finally, continuing studies of endocytosis and trafficking of MOF-based therapeutics will be required, especially for nucleic acid therapeutics, to ensure proper intracellular processing of the delivered cargo.

Going forward, it is critical that studies emphasize *in vivo* evaluation of MOF drug delivery vehicles, given the differences found *in vitro* vs. *in vivo*. Likewise, much work exists using mock drug molecules. Future work should focus on actual drug compounds to accelerate progress towards clinical applications. Further proof-of-concept studies still need to be performed for vaccines and cell-based therapies, as delivery of these species remains understudied. Also, the potential synergism of MOFs with drugs needs to be further explored 14,53,55,56. The development of MOFs for clinical applications will also require new disease targets to be explored, specifically beyond cancer, and potentially new targeting methods. The immunogenicity of MOFs likewise needs to be studied more comprehensively. The application of MOFs to drug delivery has resulted in research targeting development of therapeutics relying on catalytic nanomedicine 54 and gasotransmitters 55,56. These studies should continue as MOFs are uniquely suited for these applications.

Acknowledgments

Financial support for this work was provided in part by Michigan State University, the National Science Foundation (CBET 1802992, CBET 2029319), and the National Institutes of Health (T32GM110523, R21NS116496).

References

- (1) Zhou, H. C.; Long, J. R.; Yaghi, O. M. Introduction to Metal-Organic Frameworks. *Chem. Rev.* **2012**, *112* (2), 673–674. https://doi.org/10.1021/cr300014x.
- (2) Horcajada, P.; Serre, C.; Vallet-Regí, M.; Sebban, M.; Taulelle, F.; Férey, G. Metal-Organic Frameworks as Efficient Materials for Drug Delivery. *Angew. Chemie Int. Ed.* **2006**, *45* (36), 5974–5978. https://doi.org/10.1002/anie.200601878.
- (3) Wang, L.; Zheng, M.; Xie, Z. Nanoscale Metal-Organic Frameworks for Drug Delivery: A Conventional Platform with New Promise. *J. Mater. Chem. B* **2018**, 6 (5), 707–717. https://doi.org/10.1039/c7tb02970e.
- (4) Zheng, H.; Zhang, Y.; Liu, L.; Wan, W.; Guo, P.; Nyström, A. M.; Zou, X. One-Pot Synthesis of Metal—Organic Frameworks with Encapsulated Target Molecules and Their Applications for Controlled Drug Delivery. *J. Am. Chem. Soc.* 2016, 138 (3), 962–968. https://doi.org/10.1021/jacs.5b11720.
- (5) Vasconcelos, I. B.; Silva, T. G. da; Militão, G. C. G.; Soares, T. A.; Rodrigues, N. M.; Rodrigues, M. O.; Costa, N. B. da; Freire, R. O.; Junior, S. A. Cytotoxicity and Slow Release of the Anti-Cancer Drug Doxorubicin from ZIF-8. RSC Adv. 2012, 2 (25), 9437. https://doi.org/10.1039/c2ra21087h.
- (6) Lei, B.; Wang, M.; Jiang, Z.; Qi, W.; Su, R.; He, Z. Constructing Redox-Responsive Metal–Organic Framework Nanocarriers for Anticancer Drug Delivery. *ACS Appl. Mater. Interfaces* **2018**, *10* (19), 16698–16706. https://doi.org/10.1021/acsami.7b19693.
- (7) Wang, L.; Wang, W.; Xie, Z. Tetraphenylethylene-Based Fluorescent Coordination Polymers for Drug Delivery. *J. Mater. Chem. B* **2016**, *4* (24), 4263–4266. https://doi.org/10.1039/C6TB00952B.
- (8) Li, Y.; Zheng, Y.; Lai, X.; Chu, Y.; Chen, Y. Biocompatible Surface Modification of Nano-Scale Zeolitic Imidazolate Frameworks for Enhanced Drug Delivery. *RSC Adv.* **2018**, *8* (42), 23623–23628. https://doi.org/10.1039/C8RA03616K.
- (9) Liang, K.; Ricco, R.; Doherty, C. M.; Styles, M. J.; Bell, S.; Kirby, N.; Mudie, S.; Haylock, D.; Hill, A. J.; Doonan, C. J.; Falcaro, P. Biomimetic Mineralization of Metal-Organic Frameworks as Protective Coatings for Biomacromolecules. *Nat. Commun.* **2015**, *6* (1), 7240. https://doi.org/10.1038/ncomms8240.
- (10) Cheng, G.; Li, W.; Ha, L.; Han, X.; Hao, S.; Wan, Y.; Wang, Z.; Dong, F.; Zou, X.; Mao, Y.; Zheng, S.-Y. Self-Assembly of Extracellular Vesicle-like Metal—Organic Framework Nanoparticles for Protection and Intracellular Delivery of Biofunctional Proteins. J. Am. Chem. Soc. 2018, 140 (23), 7282–7291. https://doi.org/10.1021/jacs.8b03584.
- (11) Zhou, Y.; Liu, L.; Cao, Y.; Yu, S.; He, C.; Chen, X. A Nanocomposite Vehicle Based on Metal–Organic Framework Nanoparticle Incorporated Biodegradable Microspheres for Enhanced Oral Insulin Delivery. ACS Appl. Mater. Interfaces 2020, 12 (20), 22581–22592. https://doi.org/10.1021/acsami.0c04303.
- (12) Alsaiari, S. K.; Patil, S.; Alyami, M.; Alamoudi, K. O.; Aleisa, F. A.; Merzaban, J. S.; Li, M.; Khashab, N. M. Endosomal Escape and Delivery of CRISPR/Cas9 Genome Editing Machinery Enabled by Nanoscale Zeolitic Imidazolate

- Framework. *J. Am. Chem. Soc.* **2018**, *140* (1), 143–146. https://doi.org/10.1021/jacs.7b11754.
- (13) Poddar, A.; Pyreddy, S.; Carraro, F.; Dhakal, S.; Rassell, A.; Field, M. R.; Reddy, T. S.; Falcaro, P.; Doherty, C. M.; Shukla, R. ZIF Polymorphs for Nucleic Acid Delivery and Targeted Knockdown of Gene Expression in Prostate Cancer. **2020**, No. 1, unpublished work. https://doi.org/10.26434/chemrxiv.11807268.v1.
- (14) Joseph, N.; Lawson, H. D.; Overholt, K. J.; Damodaran, K.; Gottardi, R.; Acharya, A. P.; Little, S. R. Synthesis and Characterization of CaSr-Metal Organic Frameworks for Biodegradable Orthopedic Applications. *Sci. Rep.* **2019**, *9* (1), 13024. https://doi.org/10.1038/s41598-019-49536-9.
- (15) Li, Y.; Zhang, K.; Liu, P.; Chen, M.; Zhong, Y.; Ye, Q.; Wei, M. Q.; Zhao, H.; Tang, Z. Encapsulation of Plasmid DNA by Nanoscale Metal–Organic Frameworks for Efficient Gene Transportation and Expression. *Adv. Mater.* **2019**, *31* (29), 1–9. https://doi.org/10.1002/adma.201901570.
- (16) Luzuriaga, M. A.; Welch, R. P.; Dharmarwardana, M.; Benjamin, C. E.; Li, S.; Shahrivarkevishahi, A.; Popal, S.; Tuong, L. H.; Creswell, C. T.; Gassensmith, J. J. Enhanced Stability and Controlled Delivery of MOF-Encapsulated Vaccines and Their Immunogenic Response in Vivo. ACS Appl. Mater. Interfaces 2019, 11 (10), 9740–9746. https://doi.org/10.1021/acsami.8b20504.
- (17) Liang, K.; Richardson, J. J.; Cui, J.; Caruso, F.; Doonan, C. J.; Falcaro, P. Metal-Organic Framework Coatings as Cytoprotective Exoskeletons for Living Cells. *Adv. Mater.* **2016**, *28* (36), 7910–7914. https://doi.org/10.1002/adma.201602335.
- (18) Zhang, M.; Qiao, R.; Hu, J. Engineering Metal–Organic Frameworks (MOFS) for Controlled Delivery of Physiological Gaseous Transmitters. *Nanomaterials* **2020**, 10 (6), 1–14. https://doi.org/10.3390/nano10061134.
- (19) Eddaoudi, M.; Kim, J.; Rosi, N.; Vodak, D.; Wachter, J.; O'Keeffe, M.; Yaghi, O. M. Systematic Design of Pore Size and Functionality in Isoreticular MOFs and Their Application in Methane Storage. *Science* (80-.). 2002, 295 (5554), 469–472. https://doi.org/10.1126/science.1067208.
- (20) Yaghi, O. M.; O'Keeffe, M.; Ockwig, N. W.; Chae, H. K.; Eddaoudi, M.; Kim, J. Reticular Synthesis and the Design of New Materials. *Nature* **2003**, *423* (6941), 705–714. https://doi.org/10.1038/nature01650.
- (21) Han, Y.; Liu, W.; Huang, J.; Qiu, S.; Zhong, H.; Liu, D.; Liu, J. Cyclodextrin-Based Metal-Organic Frameworks (CD-MOFs) in Pharmaceutics and Biomedicine. *Pharmaceutics* **2018**, *10* (4). https://doi.org/10.3390/pharmaceutics10040271.
- (22) Horcajada, P.; Chalati, T.; Serre, C.; Gillet, B.; Sebrie, C.; Baati, T.; Eubank, J. F.; Heurtaux, D.; Clayette, P.; Kreuz, C.; Chang, J.-S. S.; Hwang, Y. K.; Marsaud, V.; Bories, P.-N. N.; Cynober, L.; Gil, S.; Férey, G.; Couvreur, P.; Gref, R. Porous Metal-Organic-Framework Nanoscale Carriers as a Potential Platform for Drug Deliveryand Imaging. *Nat. Mater.* 2010, 9 (2), 172–178. https://doi.org/10.1038/nmat2608.
- (23) Nasrollahi, M.; Nabipour, H.; Valizadeh, N.; Mozafari, M. *The Role of Flexibility in MOFs*; Elsevier Inc., 2020. https://doi.org/10.1016/b978-0-12-816984-1.00006-8.
- (24) McKinlay, A. C.; Eubank, J. F.; Wuttke, S.; Xiao, B.; Wheatley, P. S.; Bazin, P.; Lavalley, J.-C.; Daturi, M.; Vimont, A.; De Weireld, G.; Horcajada, P.; Serre, C.; Morris, R. E. Nitric Oxide Adsorption and Delivery in Flexible MIL-88(Fe) Metal—

- Organic Frameworks. *Chem. Mater.* **2013**, *25* (9), 1592–1599. https://doi.org/10.1021/cm304037x.
- (25) Kalmutzki, M. J.; Hanikel, N.; Yaghi, O. M. Secondary Building Units as the Turning Point in the Development of the Reticular Chemistry of MOFs. *Sci. Adv.* **2018**, *4* (10). https://doi.org/10.1126/sciadv.aat9180.
- (26) Hidalgo, T.; Alonso-Nocelo, M.; Bouzo, B. L.; Reimondez-Troitiño, S.; Abuin-Redondo, C.; De La Fuente, M.; Horcajada, P. Biocompatible Iron(lii) Carboxylate Metal-Organic Frameworks as Promising RNA Nanocarriers. *Nanoscale* **2020**, *12* (8), 4839–4845. https://doi.org/10.1039/c9nr08127e.
- (27) Pham, H.; Ramos, K.; Sua, A.; Acuna, J.; Slowinska, K.; Nguyen, T.; Bui, A.; Weber, M. D. R.; Tian, F. Tuning Crystal Structures of Iron-Based Metal-Organic Frameworks for Drug Delivery Applications. *ACS Omega* **2020**, *5* (7), 3418–3427. https://doi.org/10.1021/acsomega.9b03696.
- (28) Peng, S.; Bie, B.; Sun, Y.; Liu, M.; Cong, H.; Zhou, W.; Xia, Y.; Tang, H.; Deng, H.; Zhou, X. Metal-Organic Frameworks for Precise Inclusion of Single-Stranded DNA and Transfection in Immune Cells. *Nat. Commun.* **2018**, *9* (1), 1–10. https://doi.org/10.1038/s41467-018-03650-w.
- (29) Wang, Z.; Hu, S.; Yang, J.; Liang, A.; Li, Y.; Zhuang, Q.; Gu, J. Nanoscale Zr-Based MOFs with Tailorable Size and Introduced Mesopore for Protein Delivery. *Adv. Funct. Mater.* **2018**, *28* (16), 1707356. https://doi.org/10.1002/adfm.201707356.
- (30) Teplensky, M. H.; Fantham, M.; Poudel, C.; Hockings, C.; Lu, M.; Guna, A.; Aragones-Anglada, M.; Moghadam, P. Z.; Li, P.; Farha, O. K.; Bernaldo de Quirós Fernández, S.; Richards, F. M.; Jodrell, D. I.; Kaminski Schierle, G.; Kaminski, C. F.; Fairen-Jimenez, D. A Highly Porous Metal-Organic Framework System to Deliver Payloads for Gene Knockdown. *Chem* **2019**, *5* (11), 2926–2941. https://doi.org/10.1016/j.chempr.2019.08.015.
- (31) Zhuang, J.; Gong, H.; Zhou, J.; Zhang, Q.; Gao, W.; Fang, R. H.; Zhang, L. Targeted Gene Silencing in Vivo by Platelet Membrane–Coated Metal-Organic Framework Nanoparticles. *Sci. Adv.* **2020**, *6* (13), eaaz6108. https://doi.org/10.1126/sciadv.aaz6108.
- (32) Chen, T.-T. T.; Yi, J.-T. T.; Zhao, Y.-Y. Y.; Chu, X. Biomineralized Metal-Organic Framework Nanoparticles Enable Intracellular Delivery and Endo-Lysosomal Release of Native Active Proteins. *J. Am. Chem. Soc.* **2018**, *140* (31), 9912–9920. https://doi.org/10.1021/jacs.8b04457.
- (33) Rojas, S.; Carmona, F. J.; Maldonado, C. R.; Horcajada, P.; Hidalgo, T.; Serre, C.; Navarro, J. A. R.; Barea, E. Nanoscaled Zinc Pyrazolate Metal-Organic Frameworks as Drug-Delivery Systems. *Inorg. Chem.* **2016**, *55* (5), 2650–2663. https://doi.org/10.1021/acs.inorgchem.6b00045.
- (34) Wuttke, S.; Lismont, M.; Escudero, A.; Rungtaweevoranit, B.; Parak, W. J. Positioning Metal-Organic Framework Nanoparticles within the Context of Drug Delivery A Comparison with Mesoporous Silica Nanoparticles and Dendrimers. *Biomaterials* **2017**, *123*, 172–183. https://doi.org/10.1016/j.biomaterials.2017.01.025.
- (35) Chen, Y.; Li, P.; Modica, J. A.; Drout, R. J.; Farha, O. K. Acid-Resistant Mesoporous Metal–Organic Framework toward Oral Insulin Delivery: Protein

- Encapsulation, Protection, and Release. *J. Am. Chem. Soc.* **2018**, *140* (17), 5678–5681. https://doi.org/10.1021/jacs.8b02089.
- (36) Hou, L.; Zheng, Y.; Wang, Y.; Hu, Y.; Shi, J.; Liu, Q.; Zhang, H.; Zhang, Z. Self-Regulated Carboxyphenylboronic Acid-Modified Mesoporous Silica Nanoparticles with "Touch Switch" Releasing Property for Insulin Delivery. *ACS Appl. Mater. Interfaces* **2018**, *10* (26), 21927–21938. https://doi.org/10.1021/acsami.8b06998.
- (37) Luo, Z.; Jiang, L.; Yang, S.; Li, Z.; Soh, W. M. W.; Zheng, L.; Loh, X. J.; Wu, Y. Light-Induced Redox-Responsive Smart Drug Delivery System by Using Selenium-Containing Polymer@MOF Shell/Core Nanocomposite. *Adv. Healthc. Mater.* 2019, 8 (15), 1900406. https://doi.org/10.1002/adhm.201900406.
- (38) Orellana-Tavra, C.; Marshall, R. J.; Baxter, E. F.; Lázaro, I. A.; Tao, A.; Cheetham, A. K.; Forgan, R. S.; Fairen-Jimenez, D. Drug Delivery and Controlled Release from Biocompatible Metal–Organic Frameworks Using Mechanical Amorphization. *J. Mater. Chem. B* **2016**, *4* (47), 7697–7707. https://doi.org/10.1039/C6TB02025A.
- (39) Orellana-Tavra, C.; Baxter, E. F.; Tian, T.; Bennett, T. D.; Slater, N. K. H.; Cheetham, A. K.; Fairen-Jimenez, D. Amorphous Metal–Organic Frameworks for Drug Delivery. *Chem. Commun.* **2015**, *51* (73), 13878–13881. https://doi.org/10.1039/C5CC05237H.
- (40) Zhang, Y.; Wang, F.; Ju, E.; Liu, Z.; Chen, Z.; Ren, J.; Qu, X. Metal-Organic-Framework-Based Vaccine Platforms for Enhanced Systemic Immune and Memory Response. *Adv. Funct. Mater.* **2016**, *26* (35), 6454–6461. https://doi.org/10.1002/adfm.201600650.
- (41) Yang, X.; Tang, Q.; Jiang, Y.; Zhang, M.; Wang, M.; Mao, L. Nanoscale ATP-Responsive Zeolitic Imidazole Framework-90 as a General Platform for Cytosolic Protein Delivery and Genome Editing. *J. Am. Chem. Soc.* **2019**, *141* (9), 3782–3786. https://doi.org/10.1021/jacs.8b11996.
- (42) An, J.; Geib, S. J.; Rosi, N. L. Cation-Triggered Drug Release from a Porous Zinc-Adeninate Metal-Organic Framework. *J. Am. Chem. Soc.* **2009**, *131* (24), 8376–8377. https://doi.org/10.1021/ja902972w.
- (43) Brown, J. W.; Henderson, B. L.; Kiesz, M. D.; Whalley, A. C.; Morris, W.; Grunder, S.; Deng, H.; Furukawa, H.; Zink, J. I.; Stoddart, J. F.; Yaghi, O. M. Photophysical Pore Control in an Azobenzene-Containing Metal-Organic Framework. *Chem. Sci.* **2013**, *4* (7), 2858–2864. https://doi.org/10.1039/c3sc21659d.
- (44) Chen, W. H.; Karmi, O.; Willner, B.; Nechushtai, R.; Willner, I. Thrombin Aptamer-Modified Metal—Organic Framework Nanoparticles: Functional Nanostructures for Sensing Thrombin and the Triggered Controlled Release of Anti-Blood Clotting Drugs. Sensors (Switzerland) 2019, 19 (23). https://doi.org/10.3390/s19235260.
- (45) Chen, W.-H.; Yu, X.; Cecconello, A.; Sohn, Y. S.; Nechushtai, R.; Willner, I. Stimuli-Responsive Nucleic Acid-Functionalized Metal–Organic Framework Nanoparticles Using PH- and Metal-Ion-Dependent DNAzymes as Locks. *Chem. Sci.* **2017**, *8* (8), 5769–5780. https://doi.org/10.1039/C7SC01765K.
- (46) Chen, W. H.; Luo, G. F.; Sohn, Y. S.; Nechushtai, R.; Willner, I. Enzyme-Driven Release of Loads from Nucleic Acid–Capped Metal–Organic Framework Nanoparticles. *Adv. Funct. Mater.* **2019**, *29* (5), 1–12. https://doi.org/10.1002/adfm.201805341.

- (47) Chen, W. H.; Liao, W. C.; Sohn, Y. S.; Fadeev, M.; Cecconello, A.; Nechushtai, R.; Willner, I. Stimuli-Responsive Nucleic Acid-Based Polyacrylamide Hydrogel-Coated Metal—Organic Framework Nanoparticles for Controlled Drug Release. *Adv. Funct. Mater.* **2018**, *28* (8), 1–9. https://doi.org/10.1002/adfm.201705137.
- (48) Chen, W. H.; Yang Sung, S.; Fadeev, M.; Cecconello, A.; Nechushtai, R.; Willner, I. Targeted VEGF-Triggered Release of an Anti-Cancer Drug from Aptamer-Functionalized Metal-Organic Framework Nanoparticles. *Nanoscale* **2018**, *10* (10), 4650–4657. https://doi.org/10.1039/c8nr00193f.
- (49) Chen, W. H.; Yu, X.; Liao, W. C.; Sohn, Y. S.; Cecconello, A.; Kozell, A.; Nechushtai, R.; Willner, I. ATP-Responsive Aptamer-Based Metal–Organic Framework Nanoparticles (NMOFs) for the Controlled Release of Loads and Drugs. *Adv. Funct. Mater.* **2017**, 27 (37), 1–9. https://doi.org/10.1002/adfm.201702102.
- (50) Wang, Y.; Yan, J.; Wen, N.; Xiong, H.; Cai, S.; He, Q.; Hu, Y.; Peng, D.; Liu, Z.; Liu, Y. Metal-Organic Frameworks for Stimuli-Responsive Drug Delivery. *Biomaterials* **2020**, *230* (November 2019), 119619. https://doi.org/10.1016/j.biomaterials.2019.119619.
- (51) He, C.; Lu, K.; Liu, D.; Lin, W. Nanoscale Metal-Organic Frameworks for the Co-Delivery of Cisplatin and Pooled SiRNAs to Enhance Therapeutic Efficacy in Drug-Resistant Ovarian Cancer Cells. *J. Am. Chem. Soc.* 2014, 136 (14), 5181– 5184. https://doi.org/10.1021/ja4098862.
- (52) Su, H.; Sun, F.; Jia, J.; He, H.; Wang, A.; Zhu, G. A Highly Porous Medical Metal-Organic Framework Constructed from Bioactive Curcumin. *Chem. Commun.* **2015**, *51* (26), 5774–5777. https://doi.org/10.1039/c4cc10159f.
- (53) Liu, Z.; Peng, Y.; Xia, X.; Cao, Z.; Deng, Y.; Tang, B. Sr/PTA Metal Organic Framework as A Drug Delivery System for Osteoarthritis Treatment. *Sci. Rep.* **2019**, *9* (1), 1–7. https://doi.org/10.1038/s41598-019-54147-5.
- (54) Ding, Y.; Xu, H.; Xu, C.; Tong, Z.; Zhang, S.; Bai, Y.; Chen, Y.; Xu, Q.; Zhou, L.; Ding, H.; Sun, Z.; Yan, S.; Mao, Z.; Wang, W. A Nanomedicine Fabricated from Gold Nanoparticles-Decorated Metal–Organic Framework for Cascade Chemo/Chemodynamic Cancer Therapy. Adv. Sci. 2020, 7 (17), 2001060. https://doi.org/10.1002/advs.202001060.
- (55) Zhang, P.; Li, Y.; Tang, Y.; Shen, H.; Li, J.; Yi, Z.; Ke, Q.; Xu, H. Copper-Based Metal–Organic Framework as a Controllable Nitric Oxide-Releasing Vehicle for Enhanced Diabetic Wound Healing. ACS Appl. Mater. Interfaces 2020, 12 (16), 18319–18331. https://doi.org/10.1021/acsami.0c01792.
- (56) Chen, J.; Sheng, D.; Ying, T.; Zhao, H.; Zhang, J.; Li, Y.; Xu, H.; Chen, S. MOFs-Based Nitric Oxide Therapy for Tendon Regeneration. *Nano-Micro Lett.* **2021**, *13* (1), 1–17. https://doi.org/10.1007/s40820-020-00542-x.
- (57) Filippousi, M.; Turner, S.; Leus, K.; Siafaka, P. I.; Tseligka, E. D.; Vandichel, M.; Nanaki, S. G.; Vizirianakis, I. S.; Bikiaris, D. N.; Van Der Voort, P.; Van Tendeloo, G. Biocompatible Zr-Based Nanoscale MOFs Coated with Modified Poly(ε-Caprolactone) as Anticancer Drug Carriers. *Int. J. Pharm.* **2016**, *509* (1–2), 208–218. https://doi.org/10.1016/j.ijpharm.2016.05.048.
- (58) Zhu, W.; Guo, J.; Amini, S.; Ju, Y.; Agola, J. O.; Zimpel, A.; Shang, J.; Noureddine, A.; Caruso, F.; Wuttke, S.; Croissant, J. G.; Brinker, C. J. SupraCells:

- Living Mammalian Cells Protected within Functional Modular Nanoparticle-Based Exoskeletons. *Adv. Mater.* **2019**, *31* (25), 1900545. https://doi.org/10.1002/adma.201900545.
- (59) Yang, Y.; Hu, Q.; Zhang, Q.; Jiang, K.; Lin, W.; Yang, Y.; Cui, Y.; Qian, G. A Large Capacity Cationic Metal-Organic Framework Nanocarrier for Physiological PH Responsive Drug Delivery. *Mol. Pharm.* **2016**, *13* (8), 2782–2786. https://doi.org/10.1021/acs.molpharmaceut.6b00374.
- (60) Meng, W.; Zeng, Y.; Liang, Z.; Guo, W.; Zhi, C.; Wu, Y.; Zhong, R.; Qu, C.; Zou, R. Tuning Expanded Pores in Metal–Organic Frameworks for Selective Capture and Catalytic Conversion of Carbon Dioxide. *ChemSusChem* **2018**, *11* (21), 3751–3757. https://doi.org/10.1002/cssc.201801585.
- (61) Morris, W.; Doonan, C. J.; Furukawa, H.; Banerjee, R.; Yaghi, O. M. Crystals as Molecules: Postsynthesis Covalent Functionalization of Zeolitic Imidazolate Frameworks. J. Am. Chem. Soc. 2008, 130 (38), 12626–12627. https://doi.org/10.1021/ja805222x.
- (62) Deng, H.; Grunder, S.; Cordova, K. E.; Valente, C.; Furukawa, H.; Hmadeh, M.; Gándara, F.; Whalley, A. C.; Liu, Z.; Asahina, S.; Kazumori, H.; O'Keeffe, M.; Terasaki, O.; Stoddart, J. F.; Yaghi, O. M. Large-Pore Apertures in a Series of Metal-Organic Frameworks. Science (80-.). 2012, 336 (May), 1018–1024. https://doi.org/10.1126/science.1220131 Linking.
- (63) Cavka, J. H.; Jakobsen, S.; Olsbye, U.; Guillou, N.; Lamberti, C.; Bordiga, S.; Lillerud, K. P. A New Zirconium Inorganic Building Brick Forming Metal Organic Frameworks with Exceptional Stability. *J. Am. Chem. Soc.* **2008**, *130* (42), 13850–13851. https://doi.org/10.1021/ja8057953.
- (64) Lu, W.; Wei, Z.; Gu, Z. Y.; Liu, T. F.; Park, J.; Park, J.; Tian, J.; Zhang, M.; Zhang, Q.; Gentle, T.; Bosch, M.; Zhou, H. C. Tuning the Structure and Function of Metal-Organic Frameworks via Linker Design. *Chem. Soc. Rev.* **2014**, *43* (16), 5561–5593. https://doi.org/10.1039/c4cs00003j.
- (65) Wang, Z.; Fu, Y.; Kang, Z.; Liu, X.; Chen, N.; Wang, Q.; Tu, Y.; Wang, L.; Song, S.; Ling, D.; Song, H.; Kong, X.; Fan, C. Organelle-Specific Triggered Release of Immunostimulatory Oligonucleotides from Intrinsically Coordinated DNA-Metal-Organic Frameworks with Soluble Exoskeleton. *J. Am. Chem. Soc.* 2017, 139 (44), 15784–15791. https://doi.org/10.1021/jacs.7b07895.
- (66) Morris, W.; Briley, W. E.; Auyeung, E.; Cabezas, M. D.; Mirkin, C. A. Nucleic Acid-Metal Organic Framework (MOF) Nanoparticle Conjugates. *J. Am. Chem. Soc.* 2014, 136 (20), 7261–7264. https://doi.org/10.1021/ja503215w.
- (67) Kida, K.; Okita, M.; Fujita, K.; Tanaka, S.; Miyake, Y. Formation of High Crystalline ZIF-8 in an Aqueous Solution. *CrystEngComm* **2013**, *15* (9), 1794–1801. https://doi.org/10.1039/c2ce26847g.
- (68) Feng, L.; Wang, K. Y.; Powell, J.; Zhou, H. C. Controllable Synthesis of Metal-Organic Frameworks and Their Hierarchical Assemblies. *Matter* **2019**, *1* (4), 801–824. https://doi.org/10.1016/j.matt.2019.08.022.
- (69) Cravillon, J.; Nayuk, R.; Springer, S.; Feldhoff, A.; Huber, K.; Wiebcke, M. Controlling Zeolitic Imidazolate Framework Nano- and Microcrystal Formation: Insight into Crystal Growth by Time-Resolved in Situ Static Light Scattering. *Chem. Mater.* **2011**, *23* (8), 2130–2141. https://doi.org/10.1021/cm103571y.

- (70) Lian, X.; Erazo-Oliveras, A.; Pellois, J. P.; Zhou, H. C. High Efficiency and Long-Term Intracellular Activity of an Enzymatic Nanofactory Based on Metal-Organic Frameworks. *Nat. Commun.* 2017, 8 (1), 1–10. https://doi.org/10.1038/s41467-017-02103-0.
- (71) He, T.; Ni, B.; Xu, X.; Li, H.; Lin, H.; Yuan, W.; Luo, J.; Hu, W.; Wang, X. Competitive Coordination Strategy to Finely Tune Pore Environment of Zirconium-Based Metal-Organic Frameworks. *ACS Appl. Mater. Interfaces* **2017**, *9* (27), 22732–22738. https://doi.org/10.1021/acsami.7b06497.
- (72) Liang, W.; Chevreau, H.; Ragon, F.; Southon, P. D.; Peterson, V. K.; D'Alessandro, D. M. Tuning Pore Size in a Zirconium-Tricarboxylate Metal-Organic Framework. *CrystEngComm* **2014**, *16* (29), 6530–6533. https://doi.org/10.1039/c4ce01031k.
- (73) Jarai, B. M.; Stillman, Z.; Attia, L.; Decker, G. E.; Bloch, E. D.; Fromen, C. A. Evaluating UiO-66 Metal—Organic Framework Nanoparticles as Acid-Sensitive Carriers for Pulmonary Drug Delivery Applications. *ACS Appl. Mater. Interfaces* **2020**, *12* (35), 38989–39004. https://doi.org/10.1021/acsami.0c10900.
- (74) Butova, V. V; Soldatov, M. A.; Guda, A. A.; Lomachenko, K. A.; Lamberti, C. Metal-Organic Frameworks: Structure, Properties, Methods of Synthesis and Characterization. *Russ. Chem. Rev.* 2016, 85 (3), 280–307. https://doi.org/10.1070/rcr4554.
- (75) Illes, B.; Hirschle, P.; Barnert, S.; Cauda, V.; Wuttke, S.; Engelke, H. Exosome-Coated Metal–Organic Framework Nanoparticles: An Efficient Drug Delivery Platform. *Chem. Mater.* **2017**, *29* (19), 8042–8046. https://doi.org/10.1021/acs.chemmater.7b02358.
- (76) Nadizadeh, Z.; Naimi-Jamal, M. R.; Panahi, L. Mechanochemical Solvent-Free in Situ Synthesis of Drug-Loaded {Cu2(1,4-Bdc)2(Dabco)}n MOFs for Controlled Drug Delivery. *J. Solid State Chem.* **2018**, *259* (December 2017), 35–42. https://doi.org/10.1016/j.jssc.2017.12.027.
- (77) Souza, B. E.; Tan, J. Mechanochemical Approaches towards the in Situ Confinement of 5-FU Anti-Cancer Drug within MIL-100 (Fe) Metal-Organic Framework. *CrystEngComm* **2020**, *22* (27), 4526–4530. https://doi.org/10.1039/D0CE00638F.
- (78) Bennett, T. D.; Cao, S.; Tan, J. C.; Keen, D. A.; Bithell, E. G.; Beldon, P. J.; Friscic, T.; Cheetham, A. K. Facile Mechanosynthesis of Amorphous Zeolitic Imidazolate Frameworks. *J. Am. Chem. Soc.* **2011**, *133* (37), 14546–14549. https://doi.org/10.1021/ja206082s.
- (79) Abazari, R.; Mahjoub, A. R.; Ataei, F.; Morsali, A.; Carpenter-Warren, C. L.; Mehdizadeh, K.; Slawin, A. M. Z. Chitosan Immobilization on Bio-MOF Nanostructures: A Biocompatible PH-Responsive Nanocarrier for Doxorubicin Release on MCF-7 Cell Lines of Human Breast Cancer. *Inorg. Chem.* 2018, 57 (21), 13364–13379. https://doi.org/10.1021/acs.inorgchem.8b01955.
- (80) Mondloch, J. E.; Karagiaridi, O.; Farha, O. K.; Hupp, J. T. Activation of Metal-Organic Framework Materials. *CrystEngComm* **2013**, *15* (45), 9258–9264. https://doi.org/10.1039/c3ce41232f.
- (81) Sun, P.; Li, Z.; Wang, J.; Gao, H.; Yang, X.; Wu, S.; Liu, D.; Chen, Q. Transcellular Delivery of Messenger RNA Payloads by a Cationic Supramolecular

- MOF Platform. *Chem. Commun.* **2018**, *54* (80), 11304–11307. https://doi.org/10.1039/C8CC07047D.
- (82) Kahn, J. S.; Freage, L.; Enkin, N.; Garcia, M. A. A.; Willner, I. Stimuli-Responsive DNA-Functionalized Metal-Organic Frameworks (MOFs). *Adv. Mater.* **2017**, *29* (6), 1602782. https://doi.org/10.1002/adma.201602782.
- (83) Duan, F.; Feng, X.; Yang, X.; Sun, W.; Jin, Y.; Liu, H.; Ge, K.; Li, Z.; Zhang, J. A Simple and Powerful Co-Delivery System Based on PH-Responsive Metal-Organic Frameworks for Enhanced Cancer Immunotherapy. *Biomaterials* **2017**, 122, 23–33. https://doi.org/10.1016/j.biomaterials.2017.01.017.
- (84) Gan, N.; Sun, Q.; Zhao, L.; Tang, P.; Suo, Z.; Zhang, S.; Zhang, Y.; Zhang, M.; Wang, W.; Li, H. Protein Corona of Metal-Organic Framework Nanoparticals: Study on the Adsorption Behavior of Protein and Cell Interaction. *Int. J. Biol. Macromol.* **2019**, *140*, 709–718. https://doi.org/10.1016/j.ijbiomac.2019.08.183.
- (85) Zhuang, J.; Kuo, C. H.; Chou, L. Y.; Liu, D. Y.; Weerapana, E.; Tsung, C. K. Optimized Metal-Organic-Framework Nanospheres for Drug Delivery: Evaluation of Small-Molecule Encapsulation. *ACS Nano* **2014**, *8* (3), 2812–2819. https://doi.org/10.1021/nn406590q.
- (86) Giliopoulos, D.; Zamboulis, A.; Giannakoudakis, D.; Bikiaris, D.; Triantafyllidis, K. Polymer/Metal Organic Framework (MOF) Nanocomposites for Biomedical Applications. *Molecules* **2020**, *25* (1), 1–28. https://doi.org/10.3390/molecules25010185.
- (87) Kundu, T.; Mitra, S.; Patra, P.; Goswami, A.; Díaz Díaz, D.; Banerjee, R. Mechanical Downsizing of a Gadolinium(III)-Based Metal-Organic Framework for Anticancer Drug Delivery. *Chem. A Eur. J.* **2014**, *20* (33), 10514–10518. https://doi.org/10.1002/chem.201402244.
- (88) Shearier, E.; Cheng, P.; Zhu, Z.; Bao, J.; Hu, Y. H.; Zhao, F. Surface Defection Reduces Cytotoxicity of Zn(2-Methylimidazole) 2 (ZIF-8) without Compromising Its Drug Delivery Capacity. *RSC Adv.* **2016**, *6* (5), 4128–4135. https://doi.org/10.1039/C5RA24336J.
- (89) Teplensky, M. H.; Fantham, M.; Li, P.; Wang, T. C.; Mehta, J. P.; Young, L. J.; Moghadam, P. Z.; Hupp, J. T.; Farha, O. K.; Kaminski, C. F.; Fairen-Jimenez, D. Temperature Treatment of Highly Porous Zirconium-Containing Metal-Organic Frameworks Extends Drug Delivery Release. *J. Am. Chem. Soc.* **2017**, *139* (22), 7522–7532. https://doi.org/10.1021/jacs.7b01451.
- (90) Schneemann, A.; Bon, V.; Schwedler, I.; Senkovska, I.; Kaskel, S.; Fischer, R. A. Flexible Metal-Organic Frameworks. *Chem. Soc. Rev.* **2014**, *43* (16), 6062–6096. https://doi.org/10.1039/c4cs00101j.
- (91) Silva, I. M. P.; Carvalho, M. A.; Oliveira, C. S.; Profirio, D. M.; Ferreira, R. B.; Corbi, P. P.; Formiga, A. L. B. Enhanced Performance of a Metal-Organic Framework Analogue to MIL-101(Cr) Containing Amine Groups for Ibuprofen and Nimesulide Controlled Release. *Inorg. Chem. Commun.* **2016**, *70*, 47–50. https://doi.org/10.1016/j.inoche.2016.05.020.
- (92) Fairen-Jimenez, D.; Moggach, S. A.; Wharmby, M. T.; Wright, P. A.; Parsons, S.; Düren, T. Opening the Gate: Framework Flexibility in ZIF-8 Explored by Experiments and Simulations. *J. Am. Chem. Soc.* **2011**, *133* (23), 8900–8902. https://doi.org/10.1021/ja202154j.

- (93) Nazari, M.; Rubio-Martinez, M.; Tobias, G.; Barrio, J. P.; Babarao, R.; Nazari, F.; Konstas, K.; Muir, B. W.; Collins, S. F.; Hill, A. J.; Duke, M. C.; Hill, M. R. Metal-Organic-Framework-Coated Optical Fibers as Light-Triggered Drug Delivery Vehicles. *Adv. Funct. Mater.* **2016**, *26* (19), 3244–3249. https://doi.org/10.1002/adfm.201505260.
- (94) Wang, S.; Mcguirk, C. M.; Ross, M. B.; Wang, S.; Chen, P.; Xing, H.; Liu, Y.; Mirkin, C. A. General and Direct Method for Preparing Oligonucleotide-Functionalized Metal-Organic Framework Nanoparticles Scheme 1. (a) Schematic Representation of Solvothermal Synthesis of UiO-66 MOF Nanoparticles a; (b) DNA Modification of MOFs, Utilizing Terminal . J. Am. Chem. Soc 2017, 139, 8. https://doi.org/10.1021/jacs.7b05633.
- (95) Chen, Q.; Xu, M.; Zheng, W.; Xu, T.; Deng, H.; Liu, J. Se/Ru-Decorated Porous Metal-Organic Framework Nanoparticles for the Delivery of Pooled SiRNAs to Reversing Multidrug Resistance in Taxol-Resistant Breast Cancer Cells. *ACS Appl. Mater. Interfaces* **2017**, 9 (8), 6712–6724. https://doi.org/10.1021/acsami.6b12792.
- (96) Pinto, R. V.; Wang, S.; Tavares, S. R.; Pires, J.; Antunes, F.; Vimont, A.; Clet, G.; Daturi, M.; Maurin, G.; Serre, C.; Pinto, M. L. Tuning Cellular Biological Functions Through the Controlled Release of NO from a Porous Ti-MOF. *Angew. Chemie* **2020**, *132* (13), 5173–5181. https://doi.org/10.1002/ange.201913135.
- (97) Leng, X.; Huang, H.; Wang, W.; Sai, N.; You, L.; Yin, X.; Ni, J. Zirconium-Porphyrin PCN-222: PH-Responsive Controlled Anticancer Drug Oridonin. *Evidence-based Complement. Altern. Med.* **2018**, *2018*. https://doi.org/10.1155/2018/3249023.
- (98) Li, S.; Dharmarwardana, M.; Welch, R. P.; Benjamin, C. E.; Shamir, A. M.; Nielsen, S. O.; Gassensmith, J. J. Investigation of Controlled Growth of Metal-Organic Frameworks on Anisotropic Virus Particles. *ACS Appl. Mater. Interfaces* **2018**, *10* (21), 18161–18169. https://doi.org/10.1021/acsami.8b01369.
- (99) Poddar, A.; Conesa, J. J.; Liang, K.; Dhakal, S.; Reineck, P.; Bryant, G.; Pereiro, E.; Ricco, R.; Amenitsch, H.; Doonan, C.; Mulet, X.; Doherty, C. M.; Falcaro, P.; Shukla, R. Encapsulation, Visualization and Expression of Genes with Biomimetically Mineralized Zeolitic Imidazolate Framework-8 (ZIF-8). *Small* **2019**, *15* (36), 1902268. https://doi.org/10.1002/smll.201902268.
- (100) Luzuriaga, M. A.; Benjamin, C. E.; Gaertner, M. W.; Lee, H.; Herbert, F. C.; Mallick, S.; Gassensmith, J. J. ZIF-8 Degrades in Cell Media, Serum, and Some—but Not All—Common Laboratory Buffers. *Supramol. Chem.* **2019**, *31* (8), 485–490. https://doi.org/10.1080/10610278.2019.1616089.
- (101) Al Haydar, M.; Abid, H. R.; Sunderland, B.; Wang, S. Metal Organic Frameworks as a Drug Delivery System for Flurbiprofen. *Drug Des. Devel. Ther.* **2017**, *11*, 2685–2695. https://doi.org/10.2147/DDDT.S145716.
- (102) Pinto, R. V.; Antunes, F.; Pires, J.; Graça, V.; Brandão, P.; Pinto, M. L. Vitamin B3 Metal-Organic Frameworks as Potential Delivery Vehicles for Therapeutic Nitric Oxide. *Acta Biomater.* **2017**, *51*, 66–74. https://doi.org/10.1016/j.actbio.2017.01.039.
- (103) Abánades Lázaro, I.; Haddad, S.; Rodrigo-Muñoz, J. M.; Orellana-Tavra, C.; del Pozo, V.; Fairen-Jimenez, D.; Forgan, R. S. Mechanistic Investigation into the

- Selective Anticancer Cytotoxicity and Immune System Response of Surface-Functionalized, Dichloroacetate-Loaded, UiO-66 Nanoparticles. *ACS Appl. Mater. Interfaces* **2018**, *10* (6), 5255–5268. https://doi.org/10.1021/acsami.7b17756.
- (104) Yang, Y.; Chen, Q.; Wu, J.-P.; Kirk, T. B.; Xu, J.; Liu, Z.; Xue, W. Reduction-Responsive Codelivery System Based on a Metal–Organic Framework for Eliciting Potent Cellular Immune Response. *ACS Appl. Mater. Interfaces* **2018**, *10* (15), 12463–12473. https://doi.org/10.1021/acsami.8b01680.
- (105) Nowroozi-Nejad, Z.; Bahramian, B.; Hosseinkhani, S. Efficient Immobilization of Firefly Luciferase in a Metal Organic Framework: Fe-MIL-88(NH2) as a Mighty Support for This Purpose. *Enzyme Microb. Technol.* **2019**, *121* (October 2018), 59–67. https://doi.org/10.1016/j.enzmictec.2018.10.011.
- (106) Liang, K.; Coghlan, C. J.; Bell, S. G.; Doonan, C.; Falcaro, P. Enzyme Encapsulation in Zeolitic Imidazolate Frameworks: A Comparison between Controlled Co-Precipitation and Biomimetic Mineralisation. *Chem. Commun.* **2016**, *52* (3), 473–476. https://doi.org/10.1039/c5cc07577g.
- (107) Zhao, J.; Lu, D.; Moya, S.; Yan, H.; Qiu, M.; Chen, J. Z.; Wang, X.; Li, Y.; Pan, H.; Chen, G.; Wang, G. Bispecific T-Cell Engager (BiTE) Immunotherapy of Ovarian Cancer Based on MIL-88A MOF/MC Gene Delivery System. *Appl. Mater. Today* **2020**, *20*. https://doi.org/10.1016/j.apmt.2020.100701.
- (108) Haddad, S.; Abánades Lázaro, I.; Fantham, M.; Mishra, A.; Silvestre-Albero, J.; Osterrieth, J. W. M.; Kaminski Schierle, G. S.; Kaminski, C. F.; Forgan, R. S.; Fairen-Jimenez, D. Design of a Functionalized Metal-Organic Framework System for Enhanced Targeted Delivery to Mitochondria. *J. Am. Chem. Soc.* **2020**, *142* (14), 6661–6674. https://doi.org/10.1021/jacs.0c00188.
- (109) Tamames-Tabar, C.; Cunha, D.; Imbuluzqueta, E.; Ragon, F.; Serre, C.; Blanco-Prieto, M. J.; Horcajada, P. Cytotoxicity of Nanoscaled Metal-Organic Frameworks. *J. Mater. Chem. B* **2014**, *2* (3), 262–271. https://doi.org/10.1039/c3tb20832j.
- (110) Wuttke, S.; Zimpel, A.; Bein, T.; Braig, S.; Stoiber, K.; Vollmar, A.; Müller, D.; Haastert-Talini, K.; Schaeske, J.; Stiesch, M.; Zahn, G.; Mohmeyer, A.; Behrens, P.; Eickelberg, O.; Bölükbas, D. A.; Meiners, S. Validating Metal-Organic Framework Nanoparticles for Their Nanosafety in Diverse Biomedical Applications. *Adv. Healthc. Mater.* **2017**, *6* (2), 1–11. https://doi.org/10.1002/adhm.201600818.
- (111) Grall, R.; Hidalgo, T.; Delic, J.; Garcia-Marquez, A.; Chevillard, S.; Horcajada, P. In Vitro Biocompatibility of Mesoporous Metal (III; Fe, Al, Cr) Trimesate MOF Nanocarriers. *J. Mater. Chem. B* 2015, 3 (42), 8279–8292. https://doi.org/10.1039/c5tb01223f.
- (112) Swaminathan, S. Gadolinium Toxicity: Iron and Ferroportin as Central Targets. *Magn. Reson. Imaging* **2016**, *34* (10), 1373–1376. https://doi.org/10.1016/j.mri.2016.08.016.
- (113) Ghio, A. J.; Soukup, J. M.; Dailey, L. A.; Richards, J.; Deng, Z.; Abraham, J. L. Gadolinium Exposure Disrupts Iron Homeostasis in Cultured Cells. *J. Biol. Inorg. Chem.* **2011**, *16* (4), 567–575. https://doi.org/10.1007/s00775-011-0757-z.
- (114) Heidegger, S.; Gößl, D.; Schmidt, A.; Niedermayer, S.; Argyo, C.; Endres, S.; Bein, T.; Bourquin, C. Immune Response to Functionalized Mesoporous Silica

- Nanoparticles for Targeted Drug Delivery. *Nanoscale* **2016**, *8* (2), 938–948. https://doi.org/10.1039/c5nr06122a.
- (115) Hidalgo, T.; Giménez-Marqués, M.; Bellido, E.; Avila, J.; Asensio, M. C.; Salles, F.; Lozano, M. V.; Guillevic, M.; Simón-Vázquez, R.; González-Fernández, A.; Serre, C.; Alonso, M. J.; Horcajada, P. Chitosan-Coated Mesoporous MIL-100(Fe) Nanoparticles as Improved Bio-Compatible Oral Nanocarriers. *Sci. Rep.* **2017**, 7 (January), 1–14. https://doi.org/10.1038/srep43099.
- (116) Bellido, E.; Hidalgo, T.; Lozano, M. V.; Guillevic, M.; Simón-Vázquez, R.; Santander-Ortega, M. J.; González-Fernández, Á.; Serre, C.; Alonso, M. J.; Horcajada, P. Heparin-Engineered Mesoporous Iron Metal-Organic Framework Nanoparticles: Toward Stealth Drug Nanocarriers. *Adv. Healthc. Mater.* **2015**, *4* (8), 1246–1257. https://doi.org/10.1002/adhm.201400755.
- (117) Feng, D.; Liu, T. F.; Su, J.; Bosch, M.; Wei, Z.; Wan, W.; Yuan, D.; Chen, Y. P.; Wang, X.; Wang, K.; Lian, X.; Gu, Z. Y.; Park, J.; Zou, X.; Zhou, H. C. Stable Metal-Organic Frameworks Containing Single-Molecule Traps for Enzyme Encapsulation. *Nat. Commun.* **2015**, *6*, 1–8. https://doi.org/10.1038/ncomms6979.
- (118) Butler, K. S.; Pearce, C. J.; Nail, E. A.; Vincent, G. A.; Sava Gallis, D. F. Antibody Targeted Metal-Organic Frameworks for Bioimaging Applications. *ACS Appl. Mater. Interfaces* **2020**, *12* (28), 31217–31224. https://doi.org/10.1021/acsami.0c07835.
- (119) Chen, Y.; Zhong, H.; Wang, J.; Wan, X.; Li, Y.; Pan, W.; Li, N.; Tang, B. Catalase-like Metal–Organic Framework Nanoparticles to Enhance Radiotherapy in Hypoxic Cancer and Prevent Cancer Recurrence. *Chem. Sci.* **2019**, *10* (22), 5773–5778. https://doi.org/10.1039/C9SC00747D.
- (120) Gao, X.; Zhai, M.; Guan, W.; Liu, J.; Liu, Z.; Damirin, A. Controllable Synthesis of a Smart Multifunctional Nanoscale Metal—Organic Framework for Magnetic Resonance/Optical Imaging and Targeted Drug Delivery. *ACS Appl. Mater. Interfaces* **2017**, *9* (4), 3455–3462. https://doi.org/10.1021/acsami.6b14795.
- (121) Cherkasov, V. R.; Mochalova, E. N.; Babenyshev, A. V.; Rozenberg, J. M.; Sokolov, I. L.; Nikitin, M. P. Antibody-Directed Metal-Organic Framework Nanoparticles for Targeted Drug Delivery. *Acta Biomater.* **2020**, *103*, 223–236. https://doi.org/10.1016/j.actbio.2019.12.012.
- (122) Wang, X.-G.; Dong, Z.-Y.; Cheng, H.; Wan, S.-S.; Chen, W.-H.; Zou, M.-Z.; Huo, J.-W.; Deng, H.-X.; Zhang, X.-Z. A Multifunctional Metal–Organic Framework Based Tumor Targeting Drug Delivery System for Cancer Therapy. *Nanoscale* **2015**, *7* (38), 16061–16070. https://doi.org/10.1039/C5NR04045K.
- (123) Ding, L.; Lin, X.; Lin, Z.; Wu, Y.; Liu, X.; Liu, J.; Wu, M.; Zhang, X.; Zeng, Y. Cancer Cell-Targeted Photosensitizer and Therapeutic Protein Co-Delivery Nanoplatform Based on a Metal–Organic Framework for Enhanced Synergistic Photodynamic and Protein Therapy. *ACS Appl. Mater. Interfaces* **2020**, *12* (33), 36906–36916. https://doi.org/10.1021/acsami.0c09657.
- (124) Zhao, Q. G.; Wang, J.; Zhang, Y. P.; Zhang, J.; Tang, A. N.; Kong, D. M. A ZnO-Gated Porphyrinic Metal-Organic Framework-Based Drug Delivery System for Targeted Bimodal Cancer Therapy. *J. Mater. Chem. B* **2018**, *6* (47), 7898–7907. https://doi.org/10.1039/c8tb02663g.
- (125) Zhao, J.; Yin, F.; Ji, L.; Wang, C.; Shi, C.; Liu, X.; Yang, H.; Wang, X.; Kong, L.

- Development of a Tau-Targeted Drug Delivery System Using a Multifunctional Nanoscale Metal-Organic Framework for Alzheimer's Disease Therapy. *ACS Appl. Mater. Interfaces* **2020**, *12* (40), 44447–44458. https://doi.org/10.1021/acsami.0c11064.
- (126) Simon-Yarza, T.; Giménez-Marqués, M.; Mrimi, R.; Mielcarek, A.; Gref, R.; Horcajada, P.; Serre, C.; Couvreur, P. A Smart Metal-Organic Framework Nanomaterial for Lung Targeting. *Angew. Chemie Int. Ed.* **2017**, *56* (49), 15565–15569. https://doi.org/10.1002/anie.201707346.
- (127) Liu, Z.; Li, T.; Han, F.; Wang, Y.; Gan, Y.; Shi, J.; Wang, T.; Akhtar, M. L.; Li, Y. A Cascade-Reaction Enabled Synergistic Cancer Starvation/ROS-Mediated/Chemo-Therapy with an Enzyme Modified Fe-Based MOF. *Biomater. Sci.* **2019**, *7* (9), 3683–3692. https://doi.org/10.1039/c9bm00641a.
- (128) Abánades Lázaro, I.; Haddad, S.; Sacca, S.; Orellana-Tavra, C.; Fairen-Jimenez, D.; Forgan, R. S. Selective Surface PEGylation of UiO-66 Nanoparticles for Enhanced Stability, Cell Uptake, and PH-Responsive Drug Delivery. *Chem* 2017, 2 (4), 561–578. https://doi.org/10.1016/j.chempr.2017.02.005.
- (129) Vocelle, D.; Chan, C.; Walton, S. P. Endocytosis Controls SiRNA Efficiency: Implications for SiRNA Delivery Vehicle Design and Cell-Specific Targeting. *Nucleic Acid Ther.* **2020**, *30* (1), 22–32. https://doi.org/10.1089/nat.2019.0804.
- (130) Patil, S.; AdityaNarvekar; Puranik, A.; Jain, R.; Dandekar, P. Formulation of Therapeutic Proteins: Strategies for Developing Oral Protein Formulations. In *Innovative Dosage Forms: Design and Development at Early Stage*; 2020.
- (131) Li, S.; Dharmarwardana, M.; Welch, R. P.; Ren, Y.; Thompson, C. M.; Smaldone, R. A.; Gassensmith, J. J. Template-Directed Synthesis of Porous and Protective Core–Shell Bionanoparticles. *Angew. Chemie Int. Ed.* **2016**, *55* (36), 10691–10696. https://doi.org/10.1002/anie.201604879.
- (132) Riccò, R.; Liang, W.; Li, S.; Gassensmith, J. J.; Caruso, F.; Doonan, C.; Falcaro, P. Metal-Organic Frameworks for Cell and Virus Biology: A Perspective. *ACS Nano* **2018**, *12* (1), 13–23. https://doi.org/10.1021/acsnano.7b08056.
- (133) Mustafa, A. K.; Gadalla, M. M.; Snyder, S. H. Signaling by Gasotransmitters. *Sci. Signal.* **2009**, *2* (68), re2–re2. https://doi.org/10.1126/scisignal.268re2.
- (134) Liang, J.; Liang, K. Biocatalytic Metal–Organic Frameworks: Prospects Beyond Bioprotective Porous Matrices. *Adv. Funct. Mater.* **2020**, *30* (27), 1–24. https://doi.org/10.1002/adfm.202001648.
- (135) Ma, L.; Jiang, F.; Fan, X.; Wang, L.; He, C.; Zhou, M.; Li, S.; Luo, H.; Cheng, C.; Qiu, L. Metal–Organic-Framework-Engineered Enzyme-Mimetic Catalysts. *Adv. Mater.* **2020**, *2003065*, 1–28. https://doi.org/10.1002/adma.202003065.
- (136) Liu, C.; Yao, J.; Hu, J.; Akakuru, O. U.; Sun, S.; Chen, T.; Wu, A. Navigating NMOF-Mediated Enzymatic Reactions for Catalytic Tumor-Specific Therapy. *Mater. Horizons* **2020**. https://doi.org/10.1039/d0mh01225d.
- (137) Chen, W.-H.; Luo, G.-F.; Vázquez-González, M.; Cazelles, R.; Sohn, Y. S.; Nechushtai, R.; Mandel, Y.; Willner, I. Glucose-Responsive Metal–Organic-Framework Nanoparticles Act as "Smart" Sense-and-Treat Carriers. *ACS Nano* **2018**, *12* (8), 7538–7545. https://doi.org/10.1021/acsnano.8b03417.
- (138) Chen, H.; Li, X.; Huo, M.; Wang, L.; Chen, Y.; Chen, W.; Wang, B. Tumor-Responsive Copper-Activated Disulfiram for Synergetic Nanocatalytic Tumor

- Therapy. *Nano Res.* **2021**, *14* (1), 205–211. https://doi.org/10.1007/s12274-020-3069-1.
- (139) Harding, J. L.; Metz, J. M.; Reynolds, M. M. A Tunable, Stable, and Bioactive MOF Catalyst for Generating a Localized Therapeutic from Endogenous Sources. *Adv. Funct. Mater.* **2014**, *24* (47), 7503–7509. https://doi.org/10.1002/adfm.201402529.
- (140) Duan, Y.; Ye, F.; Huang, Y.; Qin, Y.; He, C.; Zhao, S. One-Pot Synthesis of a Metal–Organic Framework-Based Drug Carrier for Intelligent Glucose-Responsive Insulin Delivery. *Chem. Commun.* **2018**, *54* (42), 5377–5380. https://doi.org/10.1039/C8CC02708K.
- (141) Wang, L.; Zhu, H.; Shi, Y.; Ge, Y.; Feng, X.; Liu, R.; Li, Y.; Ma, Y.; Wang, L. Novel Catalytic Micromotor of Porous Zeolitic Imidazolate Framework-67 for Precise Drug Delivery. *Nanoscale* **2018**, *10* (24), 11384–11391. https://doi.org/10.1039/c8nr02493f.

Table of Contents

Abstract	2
Abbreviations	3
Introduction	5
Structures and Compositions of MOFs	5
Advantages for Drug Delivery	6
Synthesis and Characterization	8
Tuning MOF Characteristics for Drug Delivery	10
Drug Loading, Encapsulation, and Release	11
Biocompatibility, Cellular Targeting, and Uptake	15
Case Studies	17
Fine Control of MOF Pore Dimensions for Delivery of Specific Therapeutic Cargos	18
MOFs for Oral Delivery of Protein Therapeutics	19
MOFs for Long-Term, Ambient Storage of Viruses and Cells	20
MOF-based Gasotransmitter Delivery	22
Catalytic MOF-based Nanomedicine	23
Conclusions and Future Perspectives	24
Acknowledgments	24
References	25
Table of Contents	38
Table 1: MOF Applications in Drug Delivery	39
Table 2: MOF Characteristics	54
Table 3: Viability Table	63

Table 1: MOF Applications in Drug Delivery

MOF (Metal, Ligand)	MODIFICATION	CARGO (Amount loaded)	ENCAPSULATION	BIOLOGICAL TEST SYSTEM	VIABILITY TEST ¹	APPLICATION	COMMENTS - UNIQUE TO STUDY	REF
Azo-IRMOF-74-III (Mg ^{2+,} azobenzene functionalized ligand)	Functionalized - Azobenzene group	Propidium iodide (0.4 wt%)	Post Synthetic Encapsulation	-	-	Proof of concept	Light triggered release	43
Bio-MOF-1 (Zn ²⁺ , adenine, biphenyl dicarboxylate)	-	Procainamide HCl (0.22 g/g)	Post Synthetic Encapsulation - Cation Exchange	-	-	Arrhythmia	Cation stimulated release	42
Bio-MOF-13 (Co) (Co ²⁺ , adenine)	Coated - Chitosan	Doxorubicin (0.36 g/g)	Post Synthetic Encapsulation	HUVEC MCF-7	MTT (0-100 μg/mL) [†] Propidium iodide Trypan blue Annexin V	Cancer	pH responsive behavior	79
Ca-MOF (Ca ²⁺ , terephthalic acid)	-	Flurbiprofen (10 wt%)	Post Synthetic Encapsulation	-	-	Proof of concept	-	101
CaSr-MOF (Ca ²⁺ , Sr ²⁺ , and trimesic acid)	-	Dimethyloxalylglycine (>2 mg/mg)	One-pot	MC3T3 hMSC	MTT (up to 10 mg/mL)	Osteogenesis	Bone generation Dual release	14
Co-MOF (Co ²⁺ , vitamin B)	-	Nitric Oxide (2.0 µmol/mg released)	Post-Synthetic Encapsulation	HeLa HEKn	AlamarBlue (45 - 450 μg/mL)⁺	Gasotransmitter storage	BioMOF	102
Cu-MOF {Cu ₂ (1,4-BDC) ₂ (dabco)} _n {Cu ₂ (1,4-BDC-NH ₂) ₂ (dabco)} _n (bdc=benzenedicarboxylic acid, and dabco=diazabicyclooctane)	-	Ibuprofen (50 wt%)	One-pot	Simulated Body Fluid	-	Proof of concept	Solvent free synthesis Mathematical modeling	76
CuBTTri (Cu ^{2+,} 1,3,5-benzene-tris- triazole)	Incorporated into polyurethanes	-	-	-	-	Proof of concept Gasotransmitter delivery	Endogenously produced nitric oxide	139
Eu/GMP (Eu³+, guanine monophosphate)	Coated - CpG	OVA CpG	One-pot Surface-Loading	RAW264.7 Erythrocytes Mice	MTT (20-320 μg/mL)* Hemolysis assay (20-320 μg/mL)* H&E (0.1 μM of CpG and 20 μg of OVA)	Immune stimulation Cancer	Immune stimulation Dual delivery	83

Table 1: MOF Applications in Drug Delivery

FeMOF (Zr ⁴⁺ , Iron (iii) meso-tetra(4- carboxyphenyl) porphine)	Coated – (1) Gold nanoparticles (2) PEG with thiol (3) Hydrocarbon with thiol	Camptothecin (7.7%)	Post-Synthetic Encapsulation	HepG2 Balb/c mice blood Nude mice	MTT (10 ⁻¹ -10 ⁵ ng/mL) ⁺ Hemolysis assay (0.1 - 0.4 mg/mL) [*] H&E (1.00-13.0 mg/kg) ⁺ Blood chemical levels	Cancer	Multimodal therapy Iron synergy Endocytosis	54
Gd-pDBI (Gd³+,1,4-bis(5-carboxy-1H- benzimidazole-2-yI) benzene)	Ball milled	Doxorubicin (12 wt%)	Post Synthetic Encapsulation Surface-Loading	U 937 Mice Erythrocyte Lymphocytes	MTT (100 - 300 μg/mL) Trypan blue (0-200 μg/mL) Hemolysis assay (0-300 μg/mL) WST (0-300 μg/mL) LDH (0-300 μg/mL) Blood chemical levels (100-300 μg/mL)	Cancer Proof of concept	Stable in biological systems Low blood toxicity Mechanically ground	87
	Post-synthetic functionalization - ligand exchange with 4- (Methylamino) pyridine Incorporation into poly-caprolactone/gel atin scaffold	Nitric Oxide (1.67 nM/h released over 15 days)	Post-Synthetic Encapsulation	HUVEC Sprague-Dawley rats	CCK8 (cells on scaffold)* H&E	Tendon healing	Tendon Healing Copper synergy NO controlled release	56
HUSKT-1 (Cu ²⁺ , trimesic acid)	Post-synthetic functionalization - ligand exchange with 4- (Methylamino) pyridine Incorporation into poly-caprolactone/gel atin scaffold	Nitric Oxide (1.74 nM/h released over 14 days)	Post-Synthetic Encapsulation	HUVEC C57BL/6J mice	CCK8 (cells on scaffold)* H&E	Diabetic wound healing	NO controlled release Copper synergy Immune response	55
	Coated - PEG	Disulfiram (2.41 wt%)	Post-Synthetic Encapsulation	4T1 Female Kunming mice Balb/c nude mice	CCK8 (0 - 100 µg/mL)⁺ Calcein AM H&E, Blood chemical levels, weight (0 - 20 mg/kg)	Cancer	Multimodal therapy Copper synergy Catalytic nanomedicine	138

Table 1: MOF Applications in Drug Delivery

Medi-MOF-1 (Zn ²⁺ , curcumin)	-	Ibuprofen (0.24 g/g)	Post Synthetic Encapsulation	BxPC-3	MTT (0-50 μg/mL) ⁻	Cancer Proof of concept	Drug as ligand	52
Met-3-Fe (Fe ³⁺ , trimesic acid)	-	HeLa A549 HL-60 RAW264.7	Supracell construction	See cargo	CellTiter Glo 2.0	Cell protection	MOF cytoskeletons	58
MIL-100 (Cr) (Cr³+, trimesic acid)	-	Ibuprofen (0.35 g/g)	Post Synthetic Encapsulation	Simulated Body Fluid	-	-	High Loading Mathematical Modeling	2
	-	HeLa A549 HL-60 RAW264.7	Supracell construction	See cargo	CellTiter Glo 2.0	Cell protection	MOF cytoskeletons	58
MIL-100 (Fe) (Fe³+, trimesic acid)	PEGylation (pre&post synthesis) Dextran- fluorescein-biotin	Cidofovir (16.1 wt%) Busulfan (25.5 wt%) Azidothymidine triphosphate (21.2 wt%) Ibuprofen (33 wt%) Caffeine (24.2 wt%) Urea (29.2 wt%) Benzophenone 4 (15.2 wt%) Benzophenone 3 (1.5 wt%) Doxorubicin (9.1 wt%)	Post Synthetic Encapsulation	Rats J774.A1	MTT Subacute <i>in vivo</i> toxicity tests (22 to 220 mg/kg)	Anti-tumoral Anti-Viral	Multi-drug study	22
	Incorporated with SDS Coated - methoxy poly (ethylene glycol)- block-poly(L- lactide)	Insulin (35 wt%)	Post Synthetic Encapsulation	Caco-2 Balb/C mice T1D Rat	MTT (25 - 400 μg/mL) ⁺	Diabetes	Oral protein delivery Endocytosis Adsorption and biodistribution In vivo	11
	-	siRNA (8.5 wt%) miRNA	Post Synthetic Encapsulation	SW480	MTT (50 - 1200 μg/mL) [*] Human erythrocytes (15 - 500 μg/mL) [*]	Proof of concept - gene delivery	Gene delivery Green synthesis pH dependent loading	26
	-	Flurbiprofen (46 wt%)	Post Synthetic Encapsulation	-	-	Proof of concept	-	101
	Coated – Heparin	Caffeine (~43 wt%)	Post-Synthetic Encapsulation	J774.A1 HL-60	MTT (200-1200 μg/mL) ⁻	Stealth drug delivery	Immune response	116
	Coated - Chitosan	-	-	Caco-2 PBMC	MTT (200-1200 μg/mL) ⁻	-	Immune response	115

Table 1: MOF Applications in Drug Delivery

MIL-100 (Fe) (Fe³+, trimesic acid)	Coating - Carboxymethyl- dextran conjugated antibody (Her2/neu) Encapsulation - Fe nanoparticles	Doxorubicin (8%) Daunorubicin (1.5 wt%)	Post-Synthetic Encapsulation	MCF-7 BT-474 CHO SK-BR-3	MTT (0 - 300 μg/mL) ⁺	Cancer	Anti-body targeting	121
	-	GMP (30 wt%)	-	LLC-1 C57BL/6J mice	10% Weight Change (30 - 50 mg/kg) ⁺ Histology (30 - 50 mg/kg) ⁺	Proof of concept	Passive targeting	126
	-	Ibuprofen (1.4 g/g)	Post Synthetic Encapsulation	Simulated Body Fluid	-	-	High Loading Mathematical Modeling	2
MIL-101 (Cr) (Cr³+, terephthalic acid)	Functionalized - amine group (replaced ligand with 2- aminoterephthali c acid)	Ibuprofen (w/o amine – 850 mg/g) (w/ amine – 900 mg/g) Nimesulide (w/o amine – 443 mg/g) (w/ amine – 563 mg/g)	Post Synthetic Encapsulation	-	-	Proof of concept	Increased loading Mathematical modeling of release kinetics	91
	Incorporated - Selenium/rutheni um	siRNA Se (6.9 wt%) Ru (8.13 wt%)	Post Synthetic Encapsulation Surface-Loading	MCF-7/T Mice	MTT (10 μg/mL) ⁺ H&E (12 μg of siRNA)	Cancer	Multidrug resistance cancer therapy Combination therapy	95
MIL-101 (Fe) (Fe ³⁺ , terephthalic acid)	-	Flurbiprofen (37 wt%)	Post Synthetic Encapsulation	-	-	Proof of concept	-	101
	-	Cidofovir (41.9%) Azidothymidine triphosphate (42.0 wt%)	Post Synthetic Encapsulation	Rats J774.A1	MTT Subacute in vivo toxicity tests (22 to 220 mg/kg)	Anti-tumoral Anti-Viral	Multi-drug study	22
MIL-101_NH ₂ (Fe) (Fe ³⁺ , amino terephthalic acid)	-	siRNA (7.1 wt%) miRNA	Post Synthetic Encapsulation	SW480	MTT (50 - 1200 μg/mL)* Human erythrocytes (15 - 500 μg/mL)*	Proof of concept - gene delivery	Gene delivery Green synthesis pH dependent loading	26
	Coating - (1) CPG (2) Thiolated OVA	OVA (280 μg/mg) CpGs (41 μg/mg)	Surface-Loading	DC2.4 RAW264.7 APC C57BL/6 mice	CCK8 (62.5 - 1000 μg/mL) ⁺ H&E (141.5 μg/mice) [*]	Subunit vaccine	Immune response Reduction- responsive	104

Table 1: MOF Applications in Drug Delivery

MIL-101_NH ₂ (Fe) (Fe ³⁺ , amino terephthalic acid)	Post-synthetic functionalization - amine (NH2) to azide (N3) Surface Modification (1) Click-chemistry attachment of beta-cyclodextrin and thiol bridge (2) Attached RGDs peptide and PEG	Doxorubicin (13.4 wt%)	One-pot	HeLa COS7	Sulforhodamine B (SRB) (0 - 70 μg/mL) ⁺	Cancer	pH and redox responsive	122
	-	Glucose Oxidase (8.3 wt%) Camptothecin (8.6 wt%)	Post-Synthetic Encapsulation	HeLa HUVEC U87MG SMMC7721 Balb/c nude mice	ССК8 (0 - 50 µg/mL)* Н&Е	Cancer	Multimodal therapy Iron synergy	127
	-	Ibuprofen (370 mg/g)	Post Synthetic Encapsulation	NIH-3T3	MTT (50 - 2500 μg/mL) ⁻	Proof of concept	Crystal structure relation to release kinetics	27
MIL-53 (Fe) (Fe³+, terephthalic acid)	-	Busulfan (14.3 wt%) Azidothymidine triphosphate (0.24%) Ibuprofen (22 wt%) Caffeine (23.1 wt%) Urea (63.5 wt%) Benzophenone 4 (5 wt%)	Post Synthetic Encapsulation	Rats J774.A1	MTT Subacute <i>in vivo</i> toxicity tests (22 to 220 mg/kg)	Anti-tumoral Anti-Viral	Multi-drug study	22
	-	Flurbiprofen (20 wt%)	Post Synthetic Encapsulation	-	-	Proof of concept	-	101
MIL-53_NH₂ (Fe) (Fe³+, terephthalic acid)	Coated - (1) Folic acid (2) 5- carboxyfluoresce in	5-Fluorouracil	Post-Synthetic Encapsulation	MGC-803 HASMC Athymic nude mice	MTT (0 - 200 μg/mL) ⁺ Biodistribution (5 - 10 mg/kg)	Cancer	Folic acid targeting Imaging	120

Table 1: MOF Applications in Drug Delivery

-	Nitric Oxide (2.5 mmol/g)	Post-Synthetic Encapsulation	-	-	Gasotransmitter storage	Breathing structure	24
Coated - Exosome	Calcein (15.8 wt%) SBHA	Post Synthetic Encapsulation	HeLa	MTT (2-140 μg/mL) [*]	Proof of concept Cancer	Exosome coating	75
PEGylation (pre&post synthesis) Chitosan	Cidofovir (2.6 wt%) Busulfan (8.0 wt%) Azidothymidine triphosphate (0.60 wt%)	Post Synthetic Encapsulation	Rats J774.A1	MTT Subacute <i>in vivo</i> toxicity tests (22 to 220 mg/kg)	Anti-tumoral Anti-Viral	Multi-drug study	22
-	Minicircle DNA	Surface-Loading	SKOV3 293T PBMC Balb/c mice NOD/SCID mice	CCK8 (0 - 100 mg/L) ⁻ Blood chemical levels (10-20 µg/mouse) H&E (10-20 µg/mouse)	Cancer Immunotherapy	T-cell mediated cytotoxicity against human ovarian cancer	107
-	Nitric Oxide (1.6 mmol/g)	Post-Synthetic Encapsulation	-	-	Gasotransmitter storage	Breathing structure	24
-	Ibuprofen (195 mg/g)	Post Synthetic Encapsulation	NIH-3T3	MTT (50 - 2500 μg/mL) ⁻	Proof of concept	Crystal structure relation to release kinetics	27
Functionalized - NOTA Coated - DMK6240	Methylene blue (15 wt%)	Post-Synthetic Encapsulation	SH-SY5Y Sprague-Dawley rats	MTT (0 -100 μg/mL) ⁺ H&E (20 - 100 μg/rat)	Alzheimer's disease	Tau targeting	125
-	Nitric Oxide (~1.0 mmol/g)	Post-Synthetic Encapsulation	-	-	Gasotransmitter storage	Breathing structure	24
PEGylation (pre&post synthesis)	Cidofovir (14 wt%) Busulfan (9.8 wt%)	Post Synthetic Encapsulation	Rats J774.A1	MTT Subacute <i>in vivo</i> toxicity tests (22 to 220 mg/kg)	Anti-tumoral Anti-Viral	Multi-drug study	22
-	Nitric Oxide (3.0 µmol/mg released)	Post-Synthetic Encapsulation	HeLa HEKn	AlamarBlue (180 & 450 μg/mL) ⁺	Gasotransmitter delivery	High reported NO loading	96
	PEGylation (pre&post synthesis) Chitosan Functionalized - NOTA Coated - DMK6240 - PEGylation (pre&post	Coated - Exosome Calcein (15.8 wt%) SBHA Cidofovir (2.6 wt%) Busulfan (8.0 wt%) Azidothymidine triphosphate (0.60 wt%) - Minicircle DNA Minicircle DNA Nitric Oxide (1.6 mmol/g) Functionalized - NOTA Methylene blue (15 wt%) Coated - DMK6240 PEGylation (pre&post synthesis) PEGylation (pre&post synthesis) Cidofovir (2.6 wt%) Busulfan (8.0 wt%) Nitric Oxide (1.6 wt%) Methylene blue (15 wt%) Cidofovir (14 wt%) Busulfan (9.8 wt%) Nitric Oxide Nitric Oxide	Coated - Calcein (15.8 wt%) SBHA Post Synthetic Encapsulation Cidofovir (2.6 wt%) Busulfan (8.0 wt%) Azidothymidine triphosphate (0.60 wt%) - Mitric Oxide (195 mg/g) Post Synthetic Encapsulation - Ibuprofen (195 mg/g) Post Synthetic Encapsulation Functionalized - NOTA Methylene blue (15 wt%) Post-Synthetic Encapsulation Functionalized - NOTA Methylene blue (15 wt%) Post-Synthetic Encapsulation Functionalized - Nota Post-Synthetic Encapsulation	Coated - Calcein (15.8 wt%) SBHA Cidofovir (2.6 wt%) Busulfan (8.0 wt%) Synthetic Encapsulation Post Synthetic Encapsulation (2.6 wt%) Busulfan (8.0 wt%) Azidothymidine triphosphate (0.60 wt%) - Minicircle DNA Surface-Loading PBMC Balb/c mice NOD/SCID mice - Nitric Oxide (1.6 mmol/g) Post Synthetic Encapsulation PBMC Balb/c mice NOD/SCID mice - Nitric Oxide (1.6 mmol/g) Post Synthetic Encapsulation NIH-3T3 Functionalized - NOTA Methylene blue (15 wt%) Post-Synthetic Encapsulation Post-Synthetic Post-Synthetic Encapsulation Post-Synthetic Post-Synthetic Encapsulation Post-Synthetic Encapsulation Post-Synthetic Encapsulation Post-Synthetic Post-Synthetic Post-Synthetic Post-Synthetic Post-Synthetic Post-Synthetic Post-Synthetic P	Coated - Calcein (15.8 wt%) Post Synthetic Encapsulation HeLa MTT (2-140 μg/mL)'	Coated - Calcein (15.8 wt%) SBHA Post Synthetic Encapsulation Post Synthetic Encapsulation (16.8 wt%) SBHA Post Synthetic Encapsulation Post Synthetic Encapsulation (16.8 wt%) SBHA Post Synthetic Encapsulation (16.8 wt%) SBHA Post Synthetic Encapsulation (16.8 wt%) Susuafface (16.9 wt%) Post Synthetic Encapsulation (16.9 wt%) Post Synthetic Encapsulation Post Synthetic Encapsulation Post Synthetic Encapsulation Post Synthetic Encapsulation (16.9 wt%) Post Synthetic Encapsulation Post Synthetic Post Syn	Coated - Calcoin (15.8 m/s/s) Post Synthetic Encapsulation Post Synthetic Post Synthetic Encapsulation Post Synthetic Post Synthetic

Table 1: MOF Applications in Drug Delivery

MnTCCP-Hf (Hf ⁴⁺ , meso-tetrakis(4- carboxylphenyl) porphyrin- manganese)	Porphyrin conjugated with Manganese Coated - Folic acid		-	B16-F10 RBC Balb/c mice	MTT (0 - 80 μM) ⁻ Hemolysis Assay (10 - 80 μM) H&E Blood Chemical Levels (250μg/mouse)	Cancer	Folic acid targeting Catalase-like MOF Catalytic Nanomedicine	119
NCP-1-X (Zr ⁴⁺ , tetrakis(4-carboxyphenyl) ethylene acids), X = modulator amount)	Modulator - Acetic Acid	Curcumin (17.8 wt%)	Post Synthetic Encapsulation	HeLa A549 HepG2	MTT (1- 60 μg/mL) ⁻ (2.5 - 60 μg/mL) ⁺	Cancer Proof of concept	Modulators Fluorescent	7
Ni-IRMOF74-X (Ni ²⁺ , 2,5 dioxidoterephthalate, X = expanded ligand)	-	ssDNA (6.9 wt%) ssRNA	Post Synthetic Encapsulation	MCF-7 RAW264.7 THP-1 CD4+ T Cell CD4+ B Cell	Propidium Iodide MTT (0-200 μg/mL) ⁺ SRB CCK8	Gene therapy	Controlled structure Immune cell transfection Efficiency comparison to Lipo and Neofect	28
Ni-MOF (Ni ²⁺ , vitamin B)	-	Nitric Oxide (2.6 µmol/mg released)	Post-Synthetic Encapsulation	HeLa HEKn	AlamarBlue (45 - 450 μg/mL) ⁺	Gasotransmitter storage	BioMOF	102
	-	siRNA (150 pmol/mg) KALA peptide NH ₄ Cl	Post Synthetic Encapsulation	HEK-293	-	Cancer	Lipofectamine transfection comparison Gene delivery Endosomal escape	30
NU-1000 (Zr ⁴⁺ , 1,3,6,8-tetrakis(p- benzoate) pyrene)	-	Insulin (39.7 wt%)	Post Synthetic Encapsulation	Simulated physiological conditions Simulated stomach environment	-	Diabetes	Diabetes Oral protein delivery	35
	Temperature treatment	Calcein (41.6 wt%) Alpha-CHC (up to 81 wt%)	Post Synthetic Encapsulation	HeLa	MTS (0-1.50 mg/mL)*	Cancer Proof of concept	Endocytosis Extended release	89
NU-901 (Zr ⁴⁺ , 1,3,6,8-tetrakis(p- benzoate) pyrene), paraaminobenzoic acid)	Temperature treatment	Calcein (37 wt%) Alpha-CHC (up to 81 wt%)	Post Synthetic Encapsulation	HeLa	MTS (0-1.50 mg/mL)*	Cancer Proof of concept	Endocytosis Extended release	89
PCN-222 (Zr ⁴⁺ , meso-tetra (4- carboxyphenyl) porphyrin)	-	Oridonin (38.77 wt%)	Post Synthetic Encapsulation	HepG2 L02	MTT (0-160 µg/mL)⁺ LDH (0-160 µg/mL)⁺ Annexin V Propidium Iodide	Cancer	pH responsive behavior Mathematical modeling release kinetics	97

Table 1: MOF Applications in Drug Delivery

PCN-224	Coated – Di-(1- hydroxylundecyl) /Selenium/PEG/ poly (propylene glycol)/ urethane)	Doxorubicin	Post Synthetic Encapsulation	HepG2 Mice	MTT (0-50 μg/mL)* H&E (10 mg/kg body with of doxorubicin)	Cancer	Light-induced redox responsive therapy	37
(Zr ⁴⁺ , 5,10,15,20 tetrakis(4-carboxyphenyl) porphyrin)	Modulators - benzoic acid, CTAB, and PEG ZnO gating AS1411 Aptamer conjugation	Doxorubicin	Post Synthetic Encapsulation	HeLa NIH-3T3 Balb/c mice	MTT (0 - 100 μg/mL)† H&E	Cancer	Cellular Targeting pH triggered release	124
PCN-333	-	HRP (22.7 μmol/g) Cyt c (77.0 μmol/g) MP-11 (478 μmol/g)	Post Synthetic Encapsulation	-	-	Proof of concept	Enzyme immobilization	117
(Al ³⁺ , 4,4',4"-s-triazine-2,4,6- triyl-tribenzoate)	Functionalized - fluorescence	Superoxide dismutase Catalase	Post Synthetic Encapsulation	HeLa NIH-3T3 hDF	SYTOX Blue (75 μg/mL)*	Oxidative stress protection	Stabilizes enzymes Oxidative stress protection	70
Sr/PTA MOF (Sr ²⁺ , terephthalic acid)	-	Ketoprofen	Post Synthetic Encapsulation	Chondrocyte	MTT (0-800μg/mL) ⁻	Osteoarthritis	Combination therapy Proposed synergy	53
UiO-66 (Zr ⁴⁺ , terephthalic acid)	Ball Milled	Calcein (4.9 wt%)	Post Synthetic Encapsulation	HeLa	MTS (0 - 3 mg/mL) ⁻	Proof of concept	Amorphization - extended release	39
(,	-	5-Flurouracil	Post Synthetic Encapsulation	-	-	Proof of concept	Light triggered release MOF-Film Optical coating	93

Table 1: MOF Applications in Drug Delivery

	Modulator - triphenyl phosphonium and dichloroacetate	Dichloroacetate (1.2-15.5 wt%) TPP (2.3-15 wt%)	One-pot	MCF-7	MTS (0-1 mg/mL)*	Cancer Organelle specific delivery	Target mitochondria	108
	Modulator - Water (Acid-free)	Rhodamine B (~0.15 mg/mg) Dexamethasone (~0.1 mg/mg)	Post Synthetic Encapsulation	Simulated Biological Fluid MH-S A549 C57BL/6J Mice	CellTiter Glo 2.0 (1-50 μg/mL) ⁻ H&E (100μg/mouse) ⁻	Pulmonary drug delivery	Defectiveness effects Immune response	73
UiO-66 (Zr⁴+, terephthalic acid)	Modulator- Dichloroacetate Surface modification formulations: (i) surface attached folic acid and biotin (ii) click- chemistry PEG, Poly-L-lactide, poly-N- isopropylacrylam ide (iii) ligand exchange with folic acid, biotin, and heparin	Calcein (6.9-17.9 wt %) Dichloroacetate (10 - 20 wt%)	One-pot	HeLa MCF-7 HEK-293 J774 PBL	MTS (0 - 1 mg/mL) ⁺ MTT (0 - 0.50 mg/mL) ⁺	Cancer	Selective anticancer cytotoxicity Immune response	103

Table 1: MOF Applications in Drug Delivery

UiO-66-x (Zr ⁴⁺ , terephthalic acid, x = size in nm)	Modulators - Triethylamine and dodecanoic acid	Cyt C (142-160 mg/g)	Post Synthetic Encapsulation	SMMC-7721 4T1	MTT (12.5-200 μg/mL) ⁻	Proof of concept	Modulators Protein delivery	29
	Functionalized – Poly (glycidyl methacrylate) [PGMA (EA)]	mRNA	Surface-Loading	HUVEC U-87	CCK8 (Based on amine concentration)	Proof of concept - gene delivery	-	81
UiO-66-NH ₂	-	HeLa A549 HL-60 RAW264.7	Supracell construction	See cargo	CellTiter Glo 2.0	Cell protection	MOF cytoskeletons	58
(Zr⁴⁺, aminobenzene dicarboxylic acid)	Coated - (1) CpG and (2) Calcium Phosphate Modulator – Acetic acid	CpG (3.73 wt%)	Surface-Loading	RAW264.7	MTT (0-100 pM of CpG)	Immune stimulation	Immune stimulation Endocytosis	65
	Functionalized - Thrombin DNA aptamer via click chemistry	Apixaban Rhodamine 6G	Post Synthetic Encapsulation	Platelet poor plasma	-	Blood clots	Thrombin responsive DNA-gated	44
UiO-68 (Zr⁴+, amino triphenyl dicarboxylic acid)	Functionalized - (1) pH responsive DNA aptamer and AS1411 aptamer and (2) DNAzyme/substr ate units via click chemistry	Doxorubicin (52.8 µmol/g) Rhodamine 6G (62.7 µmol/g) Methylene blue (72.2 µmol/g)	Post Synthetic Encapsulation	MDA-MB-231 MCF-10A MDA-MB-231 spheroids	IncuCyte	Cancer	Multiple stimuli responsive DNA-gated	45
	Functionalized - ATP DNA aptamer via click chemistry	Camptothecin (63.9 µmol/g) Rhodamine 6G (60 µmol/g) Methylene blue (69.5 µmol/g)	Post Synthetic Encapsulation	MDA-MB-231 MCF-10A MDA-MB-231 spheroids	IncuCyte	Cancer	Enzyme drive release ATP responsive DNA-gated	46

Table 1: MOF Applications in Drug Delivery

	Coated - ATP DNA aptamer polyacrylamide hydrogel	Doxorubicin (79.1 nmol/mg) Rhodamine 6G (95.6 nmol/mg)	Post Synthetic Encapsulation	MDA-MB-231 MCF-10A MDA-MB-231 spheroids	IncuCyte	Cancer	ATP responsive DNA-gated	47
UiO-68 (Zr⁴+, amino triphenyl	Functionalized - VEGF DNA aptamer and AS1411 aptamer via click chemistry	Doxorubicin (48.1 nmol/mg) Rhodamine 6G	Post Synthetic Encapsulation	MDA-MB-231 MCF-10A MDA-MB-231 spheroids	IncuCyte	Cancer	VEGF responsive DNA-gated	48
dicarboxylic acid)	Functionalized - ATP DNA aptamer or ATP- AS1411 DNA aptamer via click chemistry	Doxorubicin Rhodamine 6G	Post Synthetic Encapsulation	MDA-MB-231 MCF-10A MDA-MB-231 spheroids	IncuCyte	Cancer	ATP responsive Cancer targeting DNA-gated	49
	-	Cisplatin (12.3 wt%) Pooled siRNA	Post Synthetic Encapsulation Surface-Loading	Skov3 PC-3 H460 A2780 A2780/CDDP	MTS (0-30µM of cisplatin) Annexin V Propidium iodide	Ovarian drug resistant cancer	Combination therapy Dual loading	51
UMCM-1 (Zn²+, amino terephthalic acid, 4,4',4"-benzene-1,3,5-triyl- tribenzoic acid, amino terephthalic acid))	Functionalized - (1) pH responsive DNA or (2) K+ responsive DNA	Rhodamine 6G	Post Synthetic Encapsulation	-	-	Proof of concept	Responsive DNA functionalization	82
				MDA-MB-468				
ZIF-8 (Zn ²⁺ , 2-methylimidazole)	-	Doxorubicin (14-20 wt%)	One-pot	MDA-MB-231 MCF-7 Primary macrophages	MTT (0 - 500μg/mL) (0.1 - 1 μg/mL) ⁺	Cancer	pH Triggered release Mesoporous	4

Table 1: MOF Applications in Drug Delivery

ZIF-8 (Zn²⁺, 2-methylimidazole)

poly(histamine aspartate-co- benzyl aspartate) (mPEG- PAsp/IM)			HeLa	MTT (12.5 - 100 μg/mL) ⁺	Cancer	pH-Triggered Release Polymer improved dispersion	8
- F	DNA BSA HSA Lysozyme HRP Ribonuclease A Hemoglobin Trypsin Lipase Insulin PQQ-GDH Urease	Biomimetic Mineralization	-	-	Protein Encapsulation	Biomimetic mineralization also shown for HKUST-1, Eu/Tb- BDC and MIL-88A Protein stabilizing/protecti ng	9
	Gelonin (17.3 wt%)	Biomimetic Mineralization	MDA-MB-231 Raw264.7 293T 3T3 SH-SY5Y CAD MCF-7 Mouse	CCK8 (0 - 100 μg/mL) ⁺ H&E (27 μg/kg body weight of gelonin)	Cancer	Mouse grafted tumor EV coating - Homotypic targeting Uptake and endocytosis	10
	siRNA CRSPR/Cas9	Biomimetic Mineralization	PC-3	МТТ	Proof of concept	Lipofectamine transfection comparison	13
Incorporated PEI (Plasmid (eGFP) (w/ PEI 3.4 wt%) (w/o PEI 2.5 wt%)	Biomimetic Mineralization One-pot	MCF-7	CCK8 (10 - 140 μg/mL)*	Proof of concept	Lipofectamine transfection comparison	15

Table 1: MOF Applications in Drug Delivery

-	Tobacco mosaic virus	Biomimetic Mineralization	Balb/C mice	H&E (10 μg, injected of cargo)	Vaccine	Vaccine protection Immune response	16
-	Baker's yeast	Biomimetic Mineralization	-	-	Cytoprotective Exoskeleton	Protects cells Controls diffusion	17
Coated - Platelet membrane	siRNA	Biomimetic Mineralization	J774 SK-BR-3 Mice	CellTiter Aqueous One Solution H&E or HRP-DAB TUNEL (injected 2 nmol siRNA)	Gene therapy	Platelet membrane coated	31
Coated - PVP	BSA (52.2 µg/mg) HSA Caspase 3 Beta-Gal	Biomimetic Mineralization	HeLa HaCat skvo3 MCF-7 HepG2	MTT (80 -150 μg/mL with BSA)	Proof of concept - Protein therapy	Delivery of native proteins	32
Coated - CpG	OVA (1.8 μmol/g)	Biomimetic Mineralization	RAW264.7 Mice	MTT (0-50 μg/mL) ⁺ CCK8 (0 - 25 μg/mL) [*] H&E (Injected 312.5 μg with cargo)	Vaccine	Vaccine platform Immune memory	40
Capping - CTAB	Fluorescein (1 wt%) Camptothecin (2 wt%)	Post Synthetic Encapsulation Surface-Loading	MCF-7	MTT (10-100μg/mL) ⁺	Proof of concept	Comparison between surface loaded and encapsulated	85
Ball milled	Hydroxyurea	-	hDF	XTT (20-1000 μg/mL)	Proof of concept	Reduced cytotoxicity	88
-	Tobacco mosaic virus	Biomimetic Mineralization	-	-	Vaccine	Vaccine Core-shell bio nanoparticle	98
-	Plasmid (IGFP)	Biomimetic Mineralization	PC-3	MTT (500 ng DNA)	Proof of concept - gene delivery	Gene delivery vehicle	99
-	Urease PVP-Urease	Biomimetic Mineralization One-pot	-	-	Proof of concept	Comparison of encapsulation methods	106
-	Tobacco mosaic virus	Biomimetic Mineralization	-	-	Proof of concept	Controlled encapsulation of virus particle	131

ZIF-8 (Zn²⁺, 2-methylimidazole)

Table 1: MOF Applications in Drug Delivery

	-	HeLa A549 HL-60 RAW264.7	Supracell construction	See cargo	CellTiter Glo 2.0	Cell protection	MOF cytoskeletons	58
ZIF-8 (Zn ²⁺ , 2-methylimidazole)	-	Cas9 (1.2 wt%) sgRNA	Biomimetic Mineralization	СНО	CCK8 (50 - 250 μg/mL)⁺	Proof of concept	Lipofectamine transfection comparison	12
	Coated - Hyaluronic acid	Chlorin e6 (7.15 wt%) Cyt c (9.01 wt%)	Biomimetic Mineralization	HeLa SMMC7721 L929 HL7702 RBC Balb/c mice	CCK8 (0-60 µg/mL)* (0 - 40 µg/mL)* Hemolysis Assay (0 - 100 µg/mL)* H&E (100 µg/mouse)*	Cancer	Photodynamic therapy	123
	-	Glucose Oxidase (17.8 µg/mg) Insulin (76.2 µg/mg) VEGF aptamer (50.2 µg/mg)	Biomimetic Mineralization	MCF-10A	AlamarBlue (100 μg/mL) ⁺	Diabetes	Glucose triggered release	137
	-	Insulin (21.5 wt%) Glucose oxidase (9.1 wt%)	One-pot	HeLa	MTT (0 - 100 μg/mL) ⁺	Diabetes	Glucose triggered release Pulsatile release	140
ZIF-67 (Co2+, 2-methylimidazole)	Coated - Iron nanoparticles	Doxorubicin (682 µg/mg)	Surface loading	-	-	Proof of concept Cancer	Micromotor	141
ZIF-90 (Zn²+, imidazole-2- carboxyaldehyde)	-	GFP RNase A-NBC Cas9 BSA SOD	Biomimetic Mineralization	HeLa	AlamarBlue (84 - 132 μg/mL) ⁻ (60 - 120 μg/mL with GFP) (150 - 250 μg/mL with RNase -NBC)	Proof of concept Cancer Gene therapy	ATP responsive Multi-application	41
ZJU-101 (Zr ⁴⁺ , 2,2'-bipyridine-5,5'- dicarboxylate with methylated pyridyl group)	Post-synthetic modification - methylation	Diclofenac sodium (0.546 g/g)	Post Synthetic Encapsulation	PC-12	MTT (20-200 μg/mL)	Anti-inflammatory	Anion exchange- controlled release	59

Table 1: MOF Applications in Drug Delivery

ZnBDP_x (Zn ²⁺ , 1,4-bis(1h-pyrazol-4-yl)-2- x-benzene, x = N, NO ₂ , NH ₂ , OH)	-	Mitoxantrone (0.2-0.5 mmol/mmol) RAPTA-C (0.11-0.55 mmol/mmol)	Post Synthetic Encapsulation	Simulated intestinal fluid	-	Proof of concept	Functionalization of MOFs Kinetics of delivery	33
Zr-Lx (Zr ⁴⁺ , x = various ligands 1-8)	Ball Milled	Alpha-CHC (3.1-31.0 wt%) Calcein (1.0-15.2 wt%)	Post Synthetic Encapsulation	HeLa	MTS (0-1.0 mg/mL) ⁻ LDH (0.25-1.0 mg/mL) ⁻	Cancer	Ball milling	38
Zr (DTBA) (Zr ⁴⁺ ,4,4'-dithiobisbenzoic acid)	-	Curcumin	Post Synthetic Encapsulation	HeLa MDA-MB-231 Balb/c Mice	MTT (0-400 μg/mL) ⁻ (0 - 40 μg/mL) [*] H&E (5 mg/kg, injected of cargo)	Cancer	Redox Responsive (G-SH) Sulfide Bridge in Structure	6

^{1. *}MOF testing done with cargo, *MOF testing done with and without cargo, MOF testing done without cargo

Table 2: MOF Characteristics

MOF (Metal, Ligand)	MORPHOLOGY	SIZE	SURFACE AREA	SYNTHESIS METHODS	PORE CHARACTERISTICS	REF
Azo-IRMOF-74-III (Mg ²⁺ , azobenzene functionalized ligand)	-	-	2410 m²/g	Solvothermal	Trans (closed) pore 8.3 Å Cis (open) pore 10.3 Å	43
Bio-MOF-1 (Zn ^{2*} , adenine, biphenyl dicarboxylate)	-	-	~1700 m²/g	Solvothermal	-	42
Bio-MOF-13 (Co) (Co ²⁺ , adenine)	Octahedral	30-90 nm 200-400 nm	935 m²/g	Solvothermal Sonochemical	Total pore volume 0.37 cm³/g Pore diameter 3.47 nm	79
Ca-MOF (Ca ²⁺ , terephthalic acid)	Rod shaped	microns	34.72 m²/g	Solvothermal	Pore width 12.33 nm Pore volume 0.10 cm³/g	101
CaSr-MOF (Ca ²⁺ , Sr ²⁺ , and trimesic acid)	Rod	Hundreds of microns	-	Non-solvothermal (water)	-	14
Co-MOF (Co ²⁺ , vitamin B)	-	-	213 m²/g	Hydrothermal	Microporous volume (0.051 cm3/g) Total porous volume (0.162 cm3/g)	102
Cu-MOF {Cu ₂ (1,4-BDC) ₂ (dabco)} _n {Cu ₂ (1,4-BDC-NH ₂) ₂ (dabco)} _n (bdc=benzenedicarboxylic acid, and dabco=diazabicyclooctane)	Nanoparticles	<100 nm	{Cu ₂ (1,4-bdc) ₂ (dabco)}n 1012.71 m²/g {Cu ₂ (1,4-bdc-NH ₂) ₂ (dabco)}n) 143.35 m²/g	Mechanochemical	{Cu ₂ (1,4-bdc) ₂ (dabco)} _n Maximum pore diameter 6.662 nm Total pore volume 0.489 cm ³ /g {C _{u2} (1,4-bdc-NH ₂) ₂ (dabco)} _n) Maximum pore diameter 19.568 nm Total pore volume 0.629 cm ³ /g	76
CuBTTri (Cu ²⁺ , 1,3,5-ben- zene-tris- triazole)	-	-	-	Solvothermal	-	139
Eu/GMP (Eu³+, guanine monophosphate)	Nanoparticles (spherical)	~30 nm	-	Non-solvothermal		83
FeMOF (Zr ⁴⁺ , Iron (iii) meso-tetra(4- carboxyphenyl) porphine)	Nanoparticles	FeMOF 50 nm	Au/FeMOF 1451 m²/g	Solvothermal	Au/FeMOF pore size 1.7 nm	54
Gd-PDBI (Gd ³⁺ ,1,4-bis(5-carboxy-1H- benzimidazole-2-yl) benzene)	Rod Shaped	Unground, 0.5 mm Ground, 120 nm	-	Solvothermal	Open Channel 1.9 nm x 1.2 nm	87

Table 2: MOF Characteristics

	Octahedral	150 nm	1194.8 m²/g	Solvothermal	Pore diameter 21.2 Å Pore volume 0.49 cm³/g	56
HUSKT-1 (Cu ²⁺ , trimesic acid)	-	100 - 300 nm	1192.3 m²/g	Solvothermal	Pore diameter 17.3 Å Pore volume 0.52 cm³/g	55
	Nanoparticles	207.3 nm	258.89 m²/g	Hydrothermal	-	138
Medi-MOF-1 (Zn ²⁺ , curcumin)	-	10 - 100 μm	3002 m²/g	Solvothermal	Pore size 0.92 nm Pore cavity 0.902 cm³/g	52
MIL-100 (Cr) (Cr³+, trimesic acid)	Cubic	,	3343 m²/g	Hydrothermal	Pore Cage 25 and 29 Å Pore Volume 8200 and 12700 Å ³ Pore Aperture 4.8x5.8 Å Pentagonal, 8.6 Å hex +pent	2
	-	<120 nm	1018.3 m²/g	Microwave	Pore 2.6 nm	11
	Spherical	<200 nm	-	Microwave	Pore Size 25 and 29 Å	22
	Nanoparticles	<200 nm	1490 m²/g	Microwave Hydrothermal	-	26
	Tetrahedral	Microns	1604.81 m²/g	Hydrothermal	Pore width 3.02 nm Pore volume 0.67 cm ³ /g	101
MIL-100 (Fe) (Fe ³⁺ , trimesic acid)	Octahedral	141-173 nm	Uncoated 1480 m²/g Coated 1530 m²/g	Hydrothermal	-	116
	Octahedral	135 - 204 nm	Uncoated 1570 m ² /g Coated 1590 m ² /g	Microwave- assisted Hydrothermal		115
	Nanoparticles	80 nm	-	Microwave	-	121
	-	130 nm	1600 m²/g	Microwave- assisted Hydrothermal	Pore window (pentagonal 5.5 Å and hexagonal 8.6 Å) Mesoporous cases (25 and 29 Å)	126

Table 2: MOF Characteristics

MIL-101 (Cr)	Cubic	,	5510 m²/g	Hydrothermal	Pore Cage 29 and 34 Å Pore Volume 12,700 - 20,600 Å ³ Pore Aperture 12 Å Pentagonal, 14.7x16 Å hex +pent	2
(Cr³+, terephthalic acid)	-	-	MIL-101 (Cr) (4420 m ² /g) NH2-MIL-101 (Cr) (2540 m ² /g)	Hydrothermal	MIL-101 (Cr) (2.50 cm ³ /g) NH2-MIL-101 (Cr) (1.50 cm ³ /g)	91
MIL-101 (Fe)	Nanoparticle	180 nm	3257 m²/g	Solvothermal	Pore size 2.25 nm Pore volume 1.49 cm ³ /g	95
(Fe ³⁺ , terephthalic acid)	Needle shape	microns	715.19 m²/g	Solvothermal	Pore width 7.33 nm Pore volume 0.55 cm³/g	101
	Octahedral	<230 nm	-	Microwave	Pore Size 29 and 34 Å	22
	Nanoparticles	<300 nm	1810 m²/g	Microwave Hydrothermal	-	26
MIL-101_NH ₂ (Fe) (Fe³+, amino terephthalic acid)	Octahedral	300 nm	Uncoated 1709 m2/g Coated 1033 m2/g	Solvothermal	-	104
	Octahedral	100-200 nm	-	Solvothermal	-	122
	Octahedral	200 nm	174 m2/g	Microwave- assisted Hydrothermal	Pore diameter 2.2 nm	127
	Rhombohedral and Spherical Nanoparticles	Microns and ~350nm	-	Solvothermal	Pore Size 8 Å	22
MIL-53 (Fe) (Fe ³⁺ , terephthalic acid)	-	-	2203 m²/g	Solvothermal	Pore volume 1400 Å ³	27
	Platelet shaped	microns	26.20 m²/g	Solvothermal	Pore width 12.30 nm Pore volume 0.06 cm³/g	101

Table 2: MOF Characteristics

MIL-53_NH ₂ (Fe) (Fe ³⁺ , amino terephthalic acid)	Nanocrystal	120 nm	198 m²/g	Facile Low- Temperature	-	120
	-	-	-	Solvothermal	-	24
MIL-88A (Fe³+, fumaric acid)	-	150-630 nm	-	Solvothermal Hydrothermal	Pore Size 6 Å	22
	Round	52 nm	218 m²/g	Microwave	Pore size 11.44 Å	75
	Spindle-like	187.8 nm	-	Microwave- assisted Hydrothermal	-	107
Mil-88B	-			Solvothermal	-	24
(Fe³⁺, terephthalic acid)	Rice	<500 nm	3042 m²/g	Solvothermal	Pore volume 1980 Å ³	27
MIL-88B_NH ₂ (Fe ³⁺ , amino terephthalic acid)	Spindle Shape	140-150 nm	-	Hydrothermal	-	125
MIL-88B_NO ₂ (Fe ³⁺ , 2-nitroterephthalic acid)	-	-	-	Solvothermal	-	24
MIL-89 (Fe³+, trans, trans-muconic acid)	Spherical nanoparticles	<260 nm	-	Solvothermal	Pore Size 6 Å	22
MIP-177 (Ti ⁴⁺ , 5,5'-methylenediisophthalic acid)	Elongated shape	100-200 nm	-	Non-Solvothermal	-	96
MnTCPP-Hf (Hf ⁴⁺ , meso-tetrakis(4- carboxylphenyl) porphyrin- magnese)	Nanoparticles	138 nm	-	Solvothermal	Pore size ~1-1.2 nm	119

Table 2: MOF Characteristics

NCP-1-x (Zr ⁴⁺ , tetrakis(4-carboxyphenyl) ethylene acids), x = modulator amount)	Octahedron Amorphous Nanoparticles	<200 nm	NCP-1 465 m ² /g NCP-1-150 810 m ² /g	Solvothermal	NCP-1-150 Pore size 4.9 Å	7
Ni-MOF (Ni ²⁺ , vitamin B)	-	-	234 m²/g	Hydrothermal	Microporous volume (0.093 cm³/g) Total porous volume (0.119 cm³/g)	102
Ni-IRMOF-74 -X (Ni ²⁺ , 2,5 dioxidoterephthalate, x = expanded ligand)	Needle Needles from spheres	Ni-IRMOF-74_II (<150 nm) Ni-IRMOF-74-III (<100 nm)	Ni-IRMOF-74-II (1930 m²/g) Ni-IRMOF-74-III (2120 m²/g) Ni-IRMOF-74-IV (1920 m²/g) Ni-IRMOF-74-V (1900 m²/g)	Solvothermal	Ni-IRMOF-74-II (Pore volume - 0.77 cm³/g) (Pore width - 1.8 nm) Ni-IRMOF-74-III (Pore volume - 0.93 cm³/g) (Pore width - 2.4 nm) Ni-IRMOF-74-IV (Pore volume 1.14 cm³/g) (Pore width - 3.0 nm) Ni-IRMOF-74-V (Pore volume 1.39 cm³/g) (Pore width 3.6 nm)	28
	-	150 nm	-	-	Pore diameter 3 nm	30
NU-1000 (Zr ⁴⁺ , 1,3,6,8-tetrakis(p-benzoate)	Rod	2 μm	~1000 m ² /g	Solvothermal	Mesopore size ~30 Å micropore size ~12 Å	35
pyrene)	2D Kagome sheets stacked	150 nm	2320 m²/g	Solvothermal	Pore volume 1.4 cm ³ /g Largest pore dimension 30 Å	89
NU-901 (Zr ⁴⁺ , 1,3,6,8-tetrakis(p-benzoate) pyrene), paraaminobenzoic acid)	Stacked diamond shaped channels	200 nm	2500 m²/g	Solvothermal	Pore volume 1.29 cm³/g Largest pore dimension 27 Å	89
PCN-222 (Zr ⁴⁺ , meso-tetra (4- carboxyphenyl) porphyrin)	Rod Shaped	5.27 μm	2476 m²/g	Solvothermal	Pore volume 1.53 cm ³ /g Pore size 1.2 nm and 3.2 nm	97
	Nanoparticles	<200 nm	-	Solvothermal	-	37
PCN-224 (Zr ⁴⁺ , 5,10,15,20 tetrakis(4- carboxyphenyl) porphyrin)	Spindle-shaped	nm	-	Solvothermal	Pore size 1.5 nm	124

Table 2: MOF Characteristics

PCN-333	Octahedron	~10 µm	4000 m ² /g	Solvothermal	Void volume 3.85 cm ³ /g	117
(Al ³⁺ , 4,4',4"-s-triazine-2,4,6-triyl- tribenzoate)	Spherical	100 nm	2793 m²/g	Solvothermal	Supertetrahedral cage 1.1 nm Dodecahedral cage 4.2 nm Hexacaidecahedral cage is 5.5 nm Void volume 2.94 cm ³ /g	70
Sr/PTA MOF (Sr ²⁺ , terephthalic acid)	Rod-like	microns	-	Solvothermal	-	53
	Amorphous	260-270 nm	1200 m²/g	Solvothermal	Pore volume 0.5 cm³/g Pore cavity 11 and 8 Å	39
	-	-	-	Solvothermal	Pore size 12.7 Å	93
UiO-66 (Zr ⁴⁺ , terephthalic acid)	Amorphous crystals	<150 nm	1200 m²/g	Solvothermal	Pore volume 0.5 cm³/g	108
	Mixed - (Spherical and cuboidal)	90 - 115 nm	-	Solvothermal	-	73
	Round	70 - 170 nm	753 - 1591 m²/g	Solvothermal	-	103
UiO-66-x (Zr ⁴⁺ , terephthalic acid, x = size in nm)	Nanoparticles	40-270 nm	mesoUiO-66-270 (1362 m²/g) mesoUiO-66-200 (1378 m²/g) mesoUiO-66-120 (1325 m²/g) mesoUiO-66-90 (1440 m²/g) mesoUiO-66-40 (1230 m²/g)	Sono- Solvothermal	Pore Diameter all = 3.4 nm mesoUiO-66-270 (Micropore volume 0.24 cm³/g, Mesopore Volume 0.65 cm³/g) mesoUiO-66-200 (Micropore volume 0.26 cm³/g, Mesopore Volume 0.75 cm³/g) mesoUiO-66-120 (Micropore volume 0.22 cm³/g, Mesopore Volume 0.69 cm³/g) mesoUiO-66-90 (Micropore volume 0.23 cm³/g, Mesopore Volume 1.20 cm³/g) mesoUiO-66-40 (Micropore volume 0.11 cm³/g, Mesopore Volume 1.29 cm³/g)	29
UiO-66-NH ₂	Spherical	26.4-41.7 nm	-	Solvothermal	-	81
(Zr ⁴⁺ , aminobenzene dicarboxylic acid)	-	154 nm	-	Solvothermal	-	65

Table 2: MOF Characteristics

	Bipyramidal	100-150 nm	1220 m²/g	Solvothermal	Pore size 1.58 nm	44
	Bipyramidal	250-300 nm	1160 m²/g	Solvothermal	Pore size 1.58 nm	45
	Bipyramidal	100-150 nm	1030 m²/g	Solvothermal	Pore size 1.45 nm	46
UiO-68 (Zr ⁴⁺ , amino triphenyl	Bipyramidal	280-350 nm	1000 m²/g	Solvothermal	Pore size 1.51 nm	47
dicarboxylic acid)	Bipyramidal	100-130 nm	1200 m²/g	Solvothermal	Pore size 1.55 nm	48
	Bipyramidal	200-250 nm	1100 m²/g	Solvothermal	Pore size 1.54 nm	49
	Hexagonal plate	100 nm x 30 nm	-	Solvothermal	Lattice fringes 1.83 nm	51
UMCM-1 (Zn ²⁺ , amino terephthalic acid, 4,4',4"-benzene-1,3,5-triyl- tribenzoic acid, amino terephthalic acid)	Rods	100s of microns	2860 m²/g	Solvothermal	Pore size 1.7 nm	82
	Dodecahedron - Irregular	70-300 nm	-	Non-solvothermal (Water)	Pore opening 3.4 Å Pore Cavity 11.6 Å	4
ZIF-8 (Zn ²⁺ , 2-methylimidazole)	-	200-300 nm		-	Pore opening 3.4 Å Pore Cavity 11.6 Å	5
(ZII , Z-Methyllimdazole)	Nanoparticle	<100 nm	-	Non-solvothermal	-	8
	Dodecahedron Nanoleaf Nanoflower Nanostar Truncated Cubes	Variable (micron)	-	Non-solvothermal (Water)	-	9
	Dodecahedron	<120 nm	-	Non-solvothermal (Water)	-	10

Table 2: MOF Characteristics

	Amorphous Nanoparticle	<250 nm	-	Non-solvothermal	-	13
	Octahedron Spheres Stars	280 nm Microns	-	Non-solvothermal (Water)	Pore 3.4 Å	15
	Nanorod	~350 nm	-	Non-solvothermal (Water)	-	16
	-	-	-	Non-solvothermal (Water)	-	17
	Nanoparticle	<200 nm	-	Non-solvothermal	-	31
ZIF-8	Nanoparticle	<100 nm	144.2 m²/g	Non-solvothermal (water)	-	32
(Zn ²⁺ , 2-methylimidazole)	Dodecahedron	200 nm	1201.7 m ² /g	Non-solvothermal	-	40
	Nanoparticles	70 nm	-	Non-solvothermal	-	85
	Amorphous	43.75 - 51.22 nm	-	Non-solvothermal	-	88
	Rod Shaped	-	-	Non-solvothermal (Water)	-	98
	Dodecahedron	<1 µm	-	Non-solvothermal (Water)	-	99
	-	-	-	Non-solvothermal (Water)	-	106
	Rod Dodecahedron	variable	-	Non-solvothermal (Water)	-	131
	Shell	80 nm	-	Non-Solvothermal (Water)	-	123
	Rhombic Dodecahedron	300 - 350 nm	-	Non-Solvothermal (Water)	-	137
	-	350-450 nm	Loaded 1219 m ² /g Not loaded 1449 m ^{2/} g	Non-Solvothermal (Water)	Loaded 0.501 cm ³ /g Not loaded 0.646 cm ³ /g	140
ZIF-67 (Co ²⁺ , 2-methylimidazole)	Dodecahedron	microns	-	Sonochemical	-	141
ZIF-90 (Zn ²⁺ , imidazole-2- carboxyaldehyde)	-	150-1000 nm	-	Non-solvothermal	-	41

Table 2: MOF Characteristics

ZJU-101 (Zr⁴+, 2,2'-bipyridine-5,5'- dicarboxylate with methylated pyridyl group)	Pooled Octahedral	~300 nm	561 m²/g	Solvothermal	Octahedral cage 1.6 nm Tetrahedral cage 1.2 nm	59
ZnBDP_x (Zn ²⁺ , 1,4-bis(1H-pyrazol-4-yl)-2-x-benzene, $x = H$, NO ₂ , NH ₂ , OH)	Tetragonal nanoparticles	ZnBDP_H (<180 nm) ZnBDP_NH ₂ (<275 nm) ZnBDP_NO ₂ (<120 nm) ZnBDP_OH (<160 nm)	ZnBDP_H (2450 m²/g) ZnBDP_NH ₂ (1420 m²/g) ZnBDP_NO ₂ (2280 m²/g) ZnBDP_OH (1020 m²/g)	Solvothermal Microwave	ZnBDP_H (Pore volume 0.959 cm³/g) ZnBDP_NH ₂ (Pore volume 0.677 cm³/g) ZnBDP_NO ₂ (Pore volume 0.822 cm³/g) ZnBDP_OH (Pore volume 0.516 cm³/g)	33
Zr-Lx (Zr⁴⁺, x = various ligands 1 -8)	Nanoparticles	Nanosized	Zr-L1 (1288 m²/g) Zr-L2 (732 m²/g) Zr-L3 (765 m²/g) Zr-L4 (916 m²/g) Zr-L5 (1492 m²/g) Zr-L6 (3010 m²/g) Zr-L7 (3634 m²/g) Zr-L8 (3494 m²/g)	Solvothermal	-	38
Zr (DTBA) (Zr ⁴⁺ ,4,4'-dithiobisbenzoic acid)	Amorphous Nanoparticle	<200 nm	-	Solvothermal	-	6

Table 3: Viability Table

CELL LINE	MOF (Metal, Ligand)	MODIFICATION	SERUM	VIABILITY TEST*	CONC. TESTED	CONC. >80% VIABLE	REF#
293T	MIL-88A (Fe) (Fe ³⁺ , fumaric acid)	-	Yes	ССК8	0 - 100 mg/L	100 mg/L	107
	HUSKT-1 (Cu²+, trimesic acid)	-	Yes	CCK8	0 - 100 μg/mL	100 μg/mL	138
4-T1 	UiO-66 -X (Zr ⁴⁺ , terephthalic acid, X = size in nm)	Modulators - Triethylamine and dodecanoic acid	Yes	MTT	0 - 200 μg/mL	200 μg/mL	29
A549	NCP-1-150 (Zr ⁴⁺ , tetrakis(4-carboxyphenyl) ethylene acids), X = modulator amount)	Modulator - Acetic Acid	Yes	MTT	1 - 60 μg/mL	60 μg/mL	7
	UiO-66 (Defectiveness 1 - 15%) (Zr ⁴⁺ , terephthalic acid)	Modulator - Water (Acid-free)	Yes	CellTiter Glo 2.	1 and 50 μg/mL	50 μg/mL	73
B16-F10	MnTCCP-Hf (Hf4+, meso-tetrakis(4- carboxylphenyl) porphyrin- Manganese)	Porphyrin conjugated with Mn Coating - Folic acid	Unknown	MTT	0 – 80 μΜ	80µM	119
BT-474	MIL-100 (Fe) (Fe ³⁺ , trimesic acid)	-	Yes	MTT	0 - 300 μg/mL	100 μg/mL	121
Caco-2	MIL-100 (Fe) (Fe³+, and trimesic acid)	-	Yes	MTT	25 - 400 μg/mL	400 μg/mL	11
Gaco-2	MIL-100 (Fe) (Fe³+, trimesic acid)	-	Yes	MTT	200-1200 μg/mL	800 μg/mL	115
СНО	ZIF-8 (Zn ²⁺ , 2-methylimidazole)	-	Yes (Reduced serum media)	ССК8	0 - 250 μg/mL	200 μg/mL	12
Chondrocyte	Sr/PTA MOF (Sr ²⁺ , terephthalic acid)	-	Yes	МТТ	0 - 800 mg/L	800 mg/L	53

Table 3: Viability Table

COS7	MIL-101_NH2 (Fe) (Fe³+, amino terephthalic acid)	Post-synthetic functionalization - amine (NH2) to azide (N3) Surface Modification (1) Click-chemistry attachment of betacyclodextrin and thiol bridge (2) Attached RGDs peptide and PEG	Yes	Sulforhodamine B (SRB)	0 - 70 μg/mL	70 μg/mL	122
DC2.4	MIL-101_NH2 (Fe) (Fe ³⁺ , amino terephthalic acid)	-	Unknown	CCK8	62.5 - 1000 µg/mL	500 μg/mL	104
Erythrocyte	Gd-pDBI (Gd³+,1,4-bis(5-carboxy-1H- benzimidazole-2-yl) benzene)	Ball milled	No (Phosphate buffered saline)	Hemolysis	0 - 300 μg/mL	300 μg/mL	87
HASMC	MIL-53_NH2 (Fe) (Fe ³⁺ , amino terephthalic acid)	Coating - (1) Folic acid (2) 5- carboxyfluorescein	Unknown	MTT	0 - 200 μg/mL	200 μg/mL	120
HEK293	UiO-66 (Zr ⁴⁺ , terephthalic acid)	Modulator- Dichloroacetate	Yes	MTS	0 - 1 mg/mL	1 mg/mL	103
	Co-MOF (Co ²⁺ , vitamin B)	-	No	AlamarBlue	45 - 450 μg/mL	180 μg/mL	102
HEKn	MIP-177 (Ti ⁴⁺ , 5,5'-methylenediisophthalic acid)	-	No	AlamarBlue	180 - 450 μg/mL	450 μg/mL	96
	Co-MOF (Co ²⁺ , vitamin B)	-	Yes	AlamarBlue	45 - 450 μg/mL	180 μg/mL	102
HeLa	MIL-101_NH2 (Fe) (Fe³+, amino terephthalic acid)	Post-synthetic functionalization - amine (NH2) to azide (N3) Surface Modification (1) Click-chemistry attachment of betacyclodextrin and thiol bridge (2) Attached RGDs peptide and PEG	Yes	Sulforhodamine B (SRB)	0 - 70 μg/mL	70 μg/mL	122

Table 3: Viability Table

HeLa

MIP-177 (Ti ⁴⁺ , 5,5'-methylenediisophthalic acid)	-	Yes	AlamarBlue	180 - 450 μg/mL	450 μg/mL	96
NCP-1-150 (Zr ⁴⁺ , tetrakis(4-carboxyphenyl) ethylene acids), X = modulator amount)	Modulator - Acetic Acid	Unknown	MTT	1 - 60 μg/mL	60 μg/mL	7
Ni-MOF (Ni ²⁺ , vitamin B)	-	Yes	AlamarBlue	45 - 450 μg/mL	270 μg/mL	102
PCN-224 (Zr ⁴⁺ , 5,10,15,20 tetrakis(4- carboxyphenyl) porphyrin)	Modulators - benzoic acid, CTAB, and PEG ZnO gating AS1411 Aptamer conjugation	Unknown	МТТ	0 - 200 μg/mL	150 μg/mL	124
UiO-66 (Zr ⁴⁺ , terephthalic acid)	-	Yes	MTS	0 - 3 mg/mL	1 mg/mL	39
UiO-66 (Zr ⁴⁺ , terephthalic acid)	-	Yes	MTS	0 - 1 mg/mL	1 mg/mL	103
ZIF-8 (Zn ²⁺ , 2-methylimidazole)	Coating - Imidazole pendent Hyaluronic acid	Yes	MTT	0 - 100 μg/mL	50 μg/mL	8
ZIF-8 (Zn ²⁺ , 2-methylimidazole)	Coating - Hyaluronic acid	Yes	CCK8	0 - 60 μg/mL	60 μg/mL	123
ZIF-8 (Zn ²⁺ , 2-methylimidazole)	-	Unknown	MTT	0 – 100 μg/mL	100 μg/mL	140
ZIF-90 (Zn ²⁺ , imidazole-2- carboxyaldehyde)	-	Yes	AlamarBlue	84 - 132 μg/mL	120 μg/mL	41
Zr (DTBA) (Zr ⁴⁺ and 4,4'-dithiobisbenzoic acid)	-	Yes	MTT	0 - 400 μg/mL	100 μg/mL	6
Zr-LX (Zr ⁴⁺ , X = various ligands 1 -7)	Ball Milled	Yes	MTS	0 - 1 mg/mL	1 mg/mL	38

Table 3: Viability Table

	FeMOF (Zr ⁴⁺ , Iron (III) meso-tetra(4-carboxyphenyl) porphine)	-	Yes	MTT	0.1 ng/mL - 100 μg/mL	10 μg/mL	54
HepG2	NCP-1-150 (Zr ⁴⁺ , tetrakis(4-carboxyphenyl) ethylene acids), X = modulator amount)	Modulator - Acetic Acid	Unknown	МТТ	1 - 60 μg/mL	60 μg/mL	7
HL-60	ZIF-8 (Zn ²⁺ , 2-methylimidazole)		Yes	MTT	0 - 25 μg/mL	25 μg/mL	5
HL7702	ZIF-8 (Zn ²⁺ , 2-methylimidazole)	Coating - Hyaluronic acid	Yes	CCK8	0 - 60 μg/mL	60 μg/mL	123
HT-29	ZIF-8 (Zn ²⁺ , 2-methylimidazole)		Yes	MTT	0 - 25 μg/mL	25 μg/mL	5
J774	UiO-66 (Zr ⁴⁺ , terephthalic acid)	-	Yes	MTS	0 - 1 mg/mL	1 mg/mL	103
J774.A1	MIL-100 (Fe) (Fe³+, trimesic acid)	-	Yes	MTT	200-1200 μg/mL	1200 μg/mL	116
L02	PCN-222 (Zr ⁴⁺ , meso-tetra (4-carboxyphenyl) porphyrin)	-	Yes	МТТ	0 - 160 μg/mL	20 μg/mL	97
L02	PCN-222 (Zr ⁴⁺ , meso-tetra (4-carboxyphenyl) porphyrin)	-	Yes	FITC-Annexin- V/Propidium lodide	0 - 160 μg/mL	160 μg/mL	97
L929	ZIF-8 (Zn ²⁺ , 2-methylimidazole)	Coating - Hyaluronic acid	Yes	CCK8	0 - 60 μg/mL	60 μg/mL	123
Lymphocytes	Gd-pDBI (Gd ³⁺ ,1,4-bis(5-carboxy-1H- benzimidazole-2-yl) benzene)	Ball milled	Unknown	WST LDH	0 - 300 μg/mL	300 μg/mL	87

Table 3: Viability Table

MCF-10A	ZIF-8 (Zn ²⁺ , 2-methylimidazole)	-	Unknown	AlamarBlue	100 μg/mL	100 μg/mL	137
	Bio-MOF-13 (Co) (Co ²⁺ , adenine)	Coated - Chitosan	Unknown	МТТ	0 - 100 μg/mL	100 μg/mL	79
	MIL-100 (Fe) (Fe ³⁺ , trimesic acid)	-	Yes	МТТ	0 - 300 μg/mL	300 μg/mL	121
	Ni-IRMOF-74 -X (Ni ²⁺ , 2,5 dioxidoterephthalate, X = expanded ligand)	-	Yes	МТТ	0 - 200 μg/mL	200 μg/mL	28
MCF-7	UiO-66 (Zr ⁴⁺ , terephthalic acid)	Modulator- Dichloroacetate	Yes	MTS	0 - 1 mg/mL	1 mg/mL	103
	ZIF-8 (Zn ²⁺ , 2-methylimidazole)	-	Yes	MTT	0 - 1 μg/mL	0.25 μg/mL	4
	ZIF-8 - 1μm (Zn²+, 2-methylimidazole)	Capping - CTAB	Unknown	MTT	0 - 100 μg/mL	100 μg/mL	85
	ZIF-8 - 70 nm (Zn ²⁺ , 2-methylimidazole)	Capping - CTAB	Unknown	MTT	0 - 100 μg/mL	10 μg/mL	85
MCF-7/T	MIL-101 (Fe) (Fe ³⁺ , terephthalic acid)	-	Yes	MTT	0 - 80 μg/mL	80 µg/mL	95

Table 3: Viability Table

	ZIF-8 (Zn ²⁺ , 2-methylimidazole)	-	Yes	MTT	0 - 1 μg/mL	0.5 μg/mL	4
MDA-MB-231	ZIF-8 (Zn ²⁺ , 2-methylimidazole)	-	Unknown	CCK8	0 - 100 μg/mL	60 μg/mL	10
	Zr (DTBA) (Zr ⁴⁺ , and 4,4'-dithiobisbenzoic acid)		Yes	МТТ	0 - 400 μg/mL	100 μg/mL	6
MDA-MB-468	ZIF-8 (Zn ²⁺ , 2-methylimidazole)	-	Yes	МТТ	0 - 1 μg/mL	1 μg/mL	4
MGC-803	MIL-53_NH2 (Fe) (Fe³+, amino terephthalic acid)	Coating - (1) Folic acid (2) 5- carboxyfluorescein	Unknown	МТТ	0 - 200 μg/mL	200 μg/mL	120
MH-S	UiO-66 (Defectiveness 1 - 15%) (Zr ⁴⁺ , terephthalic acid)	Modulator - Water (Acid-free)	Yes	CellTiter Glo 2.	1 and 50 μg/mL	50 μg/mL	73
NCI-H292	ZIF-8 (Zn ²⁺ , 2-methylimidazole)	-	Yes	MTT	0 - 25 μg/mL	25 μg/mL	5
	MIL-88 B (Fe³+, Terephthalic acid)	-	Yes	MTT	0 - 2500 μg/mL	100 μg/mL	27
NIH-3T3	PCN-224 (Zr ⁴⁺ , 5,10,15,20 tetrakis(4-carboxyphenyl) porphyrin)	Modulators - benzoic acid, CTAB, and PEG ZnO gating AS1411 Aptamer conjugation	Unknown	MTT	0 - 200 μg/mL	200 mg/L	124
PBL	UiO-66 (Zr ⁴⁺ , terephthalic acid)	-	Yes	MTS	0 - 1 mg/mL	1 mg/mL	103

Table 3: Viability Table

PC-12	ZJU-101 (Zr ⁴⁺ , 2,2'-bipyridine-5,5'- dicarboxylate with methylated pyridyl group)	Post-synthetic modification - methylation	Yes	МТТ	20 - 200 μg/mL	200 μg/mL	59
Primary macrophage	ZIF-8 (Zn ²⁺ , 2-methylimidazole)	-	Yes	МТТ	0 - 1 μg/mL	0.8 μg/mL	4
RAW264.7	ZIF-8 (Zn ²⁺ , 2-methylimidazole)	-	Unknown	MTT	0 - 50 μg/mL	25 μg/mL	40
SH-SY5Y	Mil-88B_NH2 (Fe3+, amino terephthalic acid)	Functionalized - NOTA Coated - DMK6240	Yes	МТТ	0 – 100 μg/mL	100 μg/mL	125
SMMC-7721	UiO-66 -X (Zr ⁴⁺ , terephthalic acid, X = size in nm)	Modulators - Triethylamine and dodecanoic acid	Unknown	МТТ	0 - 200 μg/mL	200 μg/mL	29
SMMC-7721	ZIF-8 (Zn ²⁺ , 2-methylimidazole)	Coating - Hyaluronic acid	Yes	CCK8	0 - 60 μg/mL	60 μg/mL	123
U 937	Gd-pDBI (Gd ³⁺ ,1,4-bis(5-carboxy-1H- benzimidazole-2-yl) benzene)	Ball milled	Yes	МТТ	0 - 300 μg/mL	200 μg/mL	87